CFD Analysis for Optimization of Vertical Axis Wind Turbine Farms.

Godwin Benedict

A thesis submitted in partial fulfillment of the requirements of the award of MSc by research, Oxford Brookes University

January 2023

Dedication

To my family for standing by my side and making me stronger.

Acknowledgements

Abstract

Vertical Axis Wind Turbines (VAWT) have gained more importance due to their compactness, adaptability and ease of installation. However, the efficiency of VAWT is much lesser than that of Horizontal Axis Wind Turbine (HAWT). Substantial research is going on to improve the efficiency of VAWT. One of the most effective methods of improving the efficiency of VAWT is to operate them on a farm rather than isolated turbines. This project deals with determining the most effective layout for a VAWT based on average performance coefficient increase when operated in a farm configuration. In order to find the optimized layout of VAWT, 2D URANS (Unsteady Reynolds Averaged Navier Stokes) CFD simulation were performed in STAR CCM+ software. Validation of the CFD simulation was done by simulating a rotor in isolation and its blade torque profile was compared to the results of published research. The validation of results proved that the blade torque profiles agree with similar studies. A new methodology has been proposed using a sliding mesh and volume controlled polyhedral meshing approach. The CPU hours for simulating 17 complete revolutions (30 seconds of flow time) of a rotor in isolation was approximately 3.5 hours (11th Gen Intel(R) Core (TM) i9-11900K @ 3.50GHz, 3504 MHz, 8 Core, 16 Logical Processor). It is also found that the current study reduces the computational time to a great extent without compromising on the accuracy. This makes the proposed methodology computationally inexpensive and faster. After validation, various configurations were simulated to identify the best possible layout for a VAWT farm. From the results the staggered configurations using a 5-rotor system proved to be the most efficient one. An increase in power output of up to 47% was observed for the same type of configuration. The V-shaped configuration consisting of five rotors yielded an increase in power output of 43%. The computational time increases exponentially as the number of rotors in the system increases. The fluid physics and mechanism which led to the increase in power output was also examined.

Table of Contents

List of Figures

Figure 1: Worldwide energy consumption in quadrillion of BTU according to EIA.

Figure 2: Top wind producing countries per capita according to European commission Brussels, .2020.

Figure 3: A gearless wind turbine rotor of HWAT [14]

Figure 4: Different types of wind turbines [13]

Figure 5: Different configurations of Wind Turbine Farm [12].

Figure 6: Flow chart showing the methodology undertaken. [45]

Figure 7: Computational domain for the CFD analysis of VAWT.D represents the diameter of the rotor as given in Table 3.

Figure 8: Figure showing the boundary conditions used.

Figure 9: Different types of meshing techniques adapted.

Figure 10: Graph showing moment coefficient value for different number

of cells for a single rotor system.

Figure 11: Graph showing moment coefficient value for different base sizes for a single rotor system.

Figure 12: Example of a VAWT array system under study.

Figure 13: Torque profile of a rotor blade, where the rotor was in isolation over an Azimuth angle of 0 to 360 degree super imposed over the torque profile of the same explained by [15] Hansen et.al.

Figure 14: Figure showing sliding mesh and overset mesh technique [11] Figure 16: Figure shows the Velocity profile of the configuration under consideration.

Figure 17: Figure shows the Vorticity profile of the configuration under consideration

Figure 18: Torque profile experienced by the rotor over the flow time.

Figure 19: Figure shows the Velocity profile of the 3D configuration under consideration: the figure is obtained from the transparent view under Star CCM+. the rotating and stationary domain be clearly seen.

Figure 20: Figure shows the Velocity profile of (sectional view) of the 3D configuration. The cross-sectional view of the velocity profile is similar to 2D.

velocity profile.

Figure 21: Torque profile experienced by the rotor (3D) over the flow time, as we can see the moment coefficient has increased promotionally comparing with figure 16.

Figure 22: Figure shows the Velocity profile of the configuration under

consideration.

Figure 23: Distribution of the rotors are arranged in the array and how they are numbered.

Figure 24: Figure shows the Vorticity profile of the configuration under

consideration.

Figure 25: Torque profile experienced by rotor 1 over the flow time. The

The position of rotor 1can be identified from figure 23.

Figure 26: Torque profile experienced by rotor 2 over the flow time. The

The position of rotor 2 can be identified from figure 23.

Figure 27: Figure shows the Velocity profile of the configuration under

consideration, 3 rotor triangle configurations.

Figure 28: Distribution of the rotors are arranged in the array and how they are numbered.

Figure 29: Figure shows the Vorticity profile of the configuration under consideration, 3 rotor triangle configurations.

Figure 30: Torque profile experienced by the rotor 1 over the flow time. Figure 31: Torque profile experienced by the rotor 2 over the flow time. Figure 32 Torque profile experienced by the rotor 3 over the flow time. The position of rotor 3 can be identified from figure 28.

Figure 33: Figure shows the Velocity profile of the configuration under consideration.

Figure 34: Distribution of the rotors are arranged in the array and how they are numbered.

Figure 35: Figure shows the Vorticity profile of the configuration under consideration.

Figure 36: Torque profile experienced by rotor 1 over the flow time.

Figure 37: Torque profile experienced by rotor 2 over the flow time.

Figure 38: Torque profile experienced by rotor 3 over the flow time.

Figure 39: Figure shows the Velocity profile of the configuration under consideration.

Figure 40: Distribution of the rotors are arranged in the array and how they are numbered.

Figure 41: Figure shows the Vorticity profile of the configuration under

consideration.

Figure 42: Torque profile experienced by rotor 1 over the flow time.

Figure 43: Torque profile experienced by rotor 2 over the flow time.

Figure 44: Torque profile experienced by rotor 3 over the flow time.

performance of each to the performance of the system. Here in this case there are five rotors, like an arrow placed at an angle of 60°

List of tables

1. Introduction

Over the past few years, countries at large have witnessed tremendous changes such as shifts in fuel prices, draining of fossil fuel reserves and unfortunate consequences of non-renewable energy sources on the environment. In this context, renewable energy sources have become an inviolable subset of energy production as they are inexhaustible, environmentally friendly and unconfined. UK government (Department of Environment, Transport and Regions) DETR has set certain goals according to the EU Kyoto obligations. UK Government's renewables has five prominent aims, and these have been reviewed in the Scottish Executive Development Departments, , Planning Advice Note (p. 1). 2 According to this document these principal aims are:

1. Encouraging the nation to attain targets for reducing the greenhouse gas emission.

2. Assisting to provide dependable, multiple and competitive energy supplies.

3. Energizing technological development so as to increase the long-term contribution from renewable resources.

4. Help the UK sustainable resources to become competitive in the international market and in turn provide more employment opportunities.

5. Involving in the growth of rural communities.

Wind energy is the most widely used renewable energy source all over the world as it is more economic. The blades of HAWTs (Horizontal Axis Wind Turbines), which face the wind directly, revolve around a horizontal rotor

shaft. They are in fact the most widely utilized form of wind turbine and are frequently found in big wind farms. While VAWTs feature blades that revolve around a horizontal axis and a vertical rotor shaft.

In terms of efficiency and duration, HAWTs are typically thought to be more efficient than VAWTs and to have longer lives. Due to their bigger blade diameters and faster rotating speeds, HAWTs have a more aerodynamic design and can harness more wind energy. As a result, they can produce more power from each unit of wind energy. HAWTs have also undergone substantial study, development, and optimization over many years, which has enhanced their dependability and performance. It is generally acknowledged that HAWTs are more effective and last longer in real-world applications. Depending on designs, site circumstances, and other reasons, the precise numbers may change.[21]

Regarding the starting torque, HAWTs normally need a faster starting wind speed than VAWTs in order to start rotating. Due to its omnidirectional design, which allows them to catch wind from any direction without the need for active yaw control, VAWTs may frequently start spinning with lower wind speeds.[22]

As for the starting torque, HAWTs typically require a higher starting However, recent studies showed that the efficiency of VAWTs increases when it is operated in a farm configuration [1][2][3]. Turbulent wakes created by the front row of horizontal axis wind turbines considerably diminish, by up to 40%, the power production of the turbines placed behind it in arrays [23]. On the other hand, smaller spacing such as 2 to 3 times the rotor diameter can be practical for VAWTs and in fact this can lead to increase in the efficiency of VAWT when used in an optimized farm configuration [6].

Most of the studies done on VAWT deal with a rotor in isolation or dipoles, which does not provide an idea of how the turbine might perform in a farm situation [1][7]. This study tries to include more rotors (up to 5) and find the most efficient way of arranging them in a layout. The studies conducted on a small number of turbines might have the drawback of results that prevent them from applying it on a larger farm. In order to accurately simulate a farm-scale situation with several turbines, this study desires to develop the most precise configuration of a Vertical Axis Wind Turbine (VAWT) layout.

Motivation of Research

A lot of research has been going on in recent times regarding the efficiency of HAWT. Studies have proved that HAWT works well in areas of high wind velocity and where the flow is uninterrupted. It is usually true that VAWTs can be more effective in low-wind locations than HAWTs, the initial torque problem needed to start spinning can be resolved through a variety of design elements. In comparison to HAWTs, VAWTs may start producing electricity at lower wind speeds, which is one of its key advantages. Because VAWTs are omnidirectional and may catch wind from any direction, they perform better than HAWTs, which must face the wind directly. Because of this, VAWTs can generate electricity from winds with erratic or changeable directions, which are frequently present in low-wind locations. [27] [28]. Simplicity of design, less vibration, reduced installation and maintenance costs are the other advantages of VAWT. Low starting torque for Vertical Axis Wind Turbines (VAWTs) might also be advantageous [22] in some circumstances. Although horizontal axis wind turbines (HAWTs) may benefit from having a high starting torque to get their revolution going, VAWTs have a distinct design and operational features that make a low starting torque useful.

Several factors make low starting torque advantageous VAWTs, including the following:

1. Start-up Performance: In comparison to HAWTs, VAWTs often have slower starting speeds. VAWTs may generate electricity even in circumstances with little wind because of their low initial torque, which enables them to start rotating at lower wind speeds. This quality is especially useful in places with variable or weak wind speeds, where HAWTs may have trouble starting and generating power.

2. Enhanced Efficiency: At slower rotating speeds, VAWTs function well. Because they don't need a lot of initial force to get going, VAWTs with low starting torque may continue to operate effectively even under low wind speeds. They can now collect electricity from a wider range of wind speeds, which can lead to an increase in total energy conversion efficiency.

3. Structural Simplicity: As opposed to HAWTs, VAWTs have a simpler mechanical construction since they don't need intricate pitch or yaw control devices. The low beginning torque enables a simpler and more reliable design, which lowers the complexity and expense of the turbine.

The previous research team from this lab, [15] Hansen et.al, also conducted CFD analysis on VAWT and found that pairs of VAWT can improve the power output by 15% compared to operating in isolation. These results provided the motivation to continue the work in the same direction. This particular study tries to include more turbines at different positions, thereby making the study more realistic compared to a farm configuration and investigates the impact of the same on the power output. The previous study was also computationally expensive as it required a powerful computer for analysis, which was one of the major drawbacks. The current study also tries to reduce the computational time and make the study more inexpensive by changing the methodology of CFD

analysis (meshing and boundary conditions).

Scope of Research

The aim of this research is to conduct a CFD analysis in order to optimize the performance of vertical axis wind turbine (VAWT) farms. Numerous studies have been conducted to investigate the performance of VAWTs, with researchers focusing on experimental and numerical analysis. These investigations aim to optimize the VAWT performance by considering factors such as the positioning relative to other turbines, as well as the geometric and operational parameters including blade shape and type.

However, there is still a research gap in conducting extensive numerical studies that incorporate a larger number of turbines in a farm configuration, considering various cluster formations. This study aims to address this gap by optimizing the vertical axis wind turbines within a farm configuration, which will provide more reliable results with industrial applications in mind.

Research Question:

What is the most optimized layout for a VAWT farm based on performance comparisons of different layouts, in order to increase the average performance coefficient of the turbines in farm configuration?

Objectives of Research

The objective of the research is to identify the optimized layout for a VAWT farm. The following steps are carried out to investigate the same.

1. To model the VAWT using CAD software (Solid Works used for this particular study).

2. To generate mesh (2D -sliding mesh) around the turbine using Star CCM+

3. To generate fluid flow field using Reynolds stress turbulence model with elliptic blending, then to determine the moment coefficient produced

4. To calculate the power coefficient and coefficient of performance from the moment coefficient

5. To find the coefficient of performance of different farm configurations following the same procedure.

6. To compare the performance of different layouts and to identify the best farm configuration.

Outline of the thesis

This thesis is demonstrated in the following direction.

- A brief literature review about the experiment and CFD investigation of Vertical Axis Wind Turbine in the similar context as explained earlier.

- The method and materials used for this research: design of the model, setting up of CFD model, numerical methodology.

- Compare and discuss the results from the CFD analysis.

- Conclusion on the study conducted, recommendations for future work.

2. Literature Review

2.1 Energy Consumption and Environmental impacts

The world we live in is going through an energy crisis like never before. Non-renewable resources of energy like the fossil fuels are being depleted repeatedly and as a result the fuel prices have reached the apex and is still continuing to increase. On the other hand, the environmental impact of the usage of fossil fuel is also increasing which is one of the major reasons for the phenomenon like global warming, caused by the emission of carbon dioxide into the atmosphere. Figure 1(a) depicts the worldwide energy consumption by different energy source, from the data, majority of the energy consumed recently comes from fossil origin – coal, natural gas and most of the liquid sources are fossil energy sources.
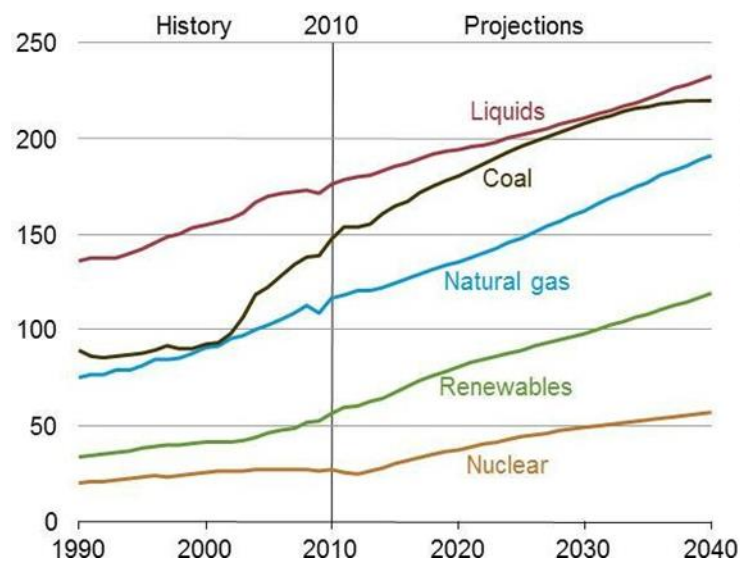
Figure 1: Worldwide energy consumption in quadrillion of BTU according to EIA.
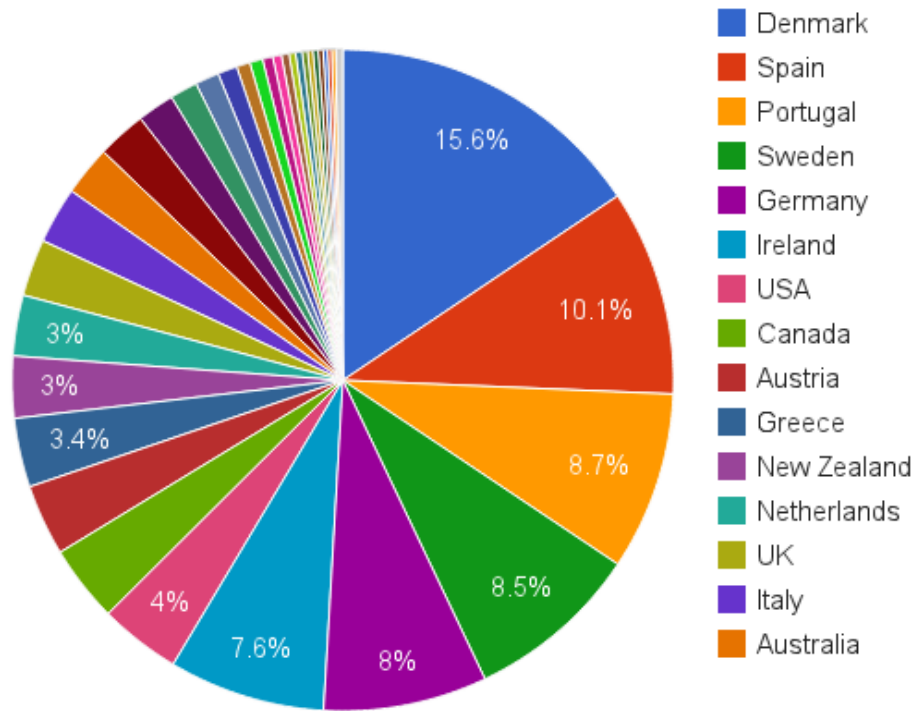
Figure 2: Top wind producing countries per capita according to European commission Brussels, .2020.

Figure 1 (b) depicts the amount of wind production across the globe in recent times, as we can see Denmark continues to be on top of the list with followed by Spain and some other European Union countries. The United Kingdom stands 13th in the list with a wind energy production capacity of only 3 %, considering the energy crisis and the potential that the nation poses in case of wind energy production, this value should be considered below par.

2 .1.1 The EU's policy framework and legislation for nature, biodiversity and climate change

The European commission approved the EU biodiversity strategy in May 2020. Overexploitation of land and sea, unsustainable use of natural resources and pollution were identified as the main cause of biodiversity loss. Biodiversity considerations are indispensable part of the economic growth strategy of the European Union. And emphasizes the necessity of having more renewable sources of energy to cope up with climatic change and biodiversity loss.

Intergovernmental Science-Policy Platform on Biodiversity and Ecosystem Services (IPBES), 2019 also stresses the need of ecosystem conservation. The report says that over the last fifty years the rate of global change of nature has increased by large scale and this was the main cause of biodiversity loss. Climatic change is ranked as third main direct driver of biodiversity loss, explaining the importance of renewable energy, especially wind energy in conservation of nature.

2.1.2 The Birds and Habitats Directives

The EU nature and biodiversity policy explains the importance of The Birds and Habitats Directives. This common legislative structure permits all EU nations to work together and conserve Europe's most vulnerable habitats. These directives are applicable for both land and marine territories in Europe. The main goal is to make sure the habitat types and species are protected all over the European Union. These goals are achieved by the following measures: preserving the core sites and habitats listed by the birds directives. These sites constitute two thousand networks all over EU, which include 27000 sites on land and sea. However, the directives do not exclude the development of wind farms near the sites.

2.2 Wind Energy

Wind is generated due to pressure difference in the atmosphere. As we know particles tend to move from higher pressure to lower pressure, similarly 3 m in the atmosphere also moves from high pressure end to low pressure end, subjected to Coriolis effect.[29][30]. In a revolving frame of reference, like the Earth, the Coriolis effect is a phenomenon that impacts the velocity of things, including air molecules. It results from the deflection that the rotation of the Earth's axis causes in moving objects. The Coriolis effect has a substantial impact on how the patterns of global atmospheric circulation are shaped in the setting of air motion and pressure fields. The uneven heating of the Earth's surface by the Sun, which produces temperature and pressure gradients, is the main cause of atmospheric circulation. The Coriolis effect occurs as air molecules travel from high-pressure areas to low-pressure areas. An item travelling over the surface of the Earth seems to be moving because of the Earth's rotation. In the Northern Hemisphere, it was deflected to the right, and in the Southern Hemisphere, to the left. This deflection is inversely proportional to the latitude and speed of the moving item.

The Coriolis effect has an impact on how pressure systems, such as high- and low-pressure zones, arise and how air masses flow between them. Air travelling from a high to a low-pressure area in the Northern Hemisphere is diverted to the right, causing clockwise circulation around the high-pressure area and anticlockwise circulation around the low-pressure area. The circulation is inverted in the Southern Hemisphere. Trade winds, dominant westerlies, and polar winds are just a few examples of the unique wind patterns that are created as a result of the Coriolis effect's deflection. Mechanical energy can be produced by using wind, which in turn can be used to generate electrical energy.

2.3 Wind Turbines

Wind Turbines are used to convert Kinetic energy of the wind to Mechanical energy, which is then converted into electrical energy. [4]. Wind turbines are generally classified into large scale wind turbines and small-scale wind turbines. Large scale wind turbines have a rotor diameter of 50 m to 100 m and generate power of 1 to 3 MW. Whereas small scale wind turbines have diameter ranging from 3m to 10 m and a power of 14 to 20 KW.

Based on the axis of rotation wind turbines can be classified into HAWT and VAWT. When rotor axis is in vertical direction such wind turbines are called VAWT. These turbines do not have the ability to self-start and yaw. But they are easy to maintain, the generator is paced on ground and the height of operation is very low. Vertical axis wind turbines (VAWTs) have a lower height of operation than horizontal axis wind turbines (HAWTs). Blades and generators are often found close to or at ground level in VAWTs.

The size and design of the VAWT will determine the precise height of operation. However, VAWTs are generally praised for being small and low-profile, which enables them to operate at comparatively lower heights than HAWTs.

This lower height has the benefit of making maintenance and inspection activities easier. Since the generator and gearbox of the VAWT are situated close to the ground, technicians may access these parts easily and it is easier to maintain them. This decreases the need for specialized equipment, such cranes or high scaffolding, which saves money and time when used for maintenance activities. The efficiency of VAWT ranges up to 50%. When rotor axis is in horizontal direction it is called HAWT. These turbines have the yawing mechanism and capability to self-start. The height of these turbines is more as the performance depends on the wind direction. The efficiency of these turbines ranges up to 70%.

2.4 HAWTs

As mentioned earlier the axis of HWAT is horizontal. Figure (2) shows a large scale HAWT, with blade upwind, these types of wind turbine generates majority of the worlds wind energy these days. Large-scale Horizontal Axis Wind turbines (HAWTs) can have some effects on the weather, but it's crucial to remember that the overall effects are complicated and can change based on several variables including the turbine's design, location, and surrounding circumstances. Instead of only attempting to lessen the effects of climate change, efforts to reduce the size of HAWTs are frequently motivated by aspects including cost-effectiveness, convenience of installation, and local limits.[35]. Table shows the main differences between HAWTs and VAWTs [22][36][37]

Figure 3: A gearless wind turbine rotor of HWAT [14]

Table 1: Differences between HAWTs and VAWTs [22][36][37]

	HAWTs	VAWTs
Advantages	- High efficiency	- Omnidirectional wind capture
	- Established technology	- No need for yaw mechanism
	- Lower noise levels	- Lower sensitivity to wind direction
	- Better performance in turbulent conditions	- Simpler maintenance and installation
		- Potential for aesthetic integration
Disadvantages	- Requires yaw mechanism for wind tracking	- Lower overall efficiency
	- Limited placement options	- Higher drag and lower starting torque
		- Complex maintenance for some designs

2.5 Types of VAWT

There are mainly three types of VAWT, they are Darrieus , Savonius, and H- Rotor type wind turbine. This project deals with the H-Rotor type of VAWT which is the simplest and most energy efficient type of VAWT [8]. The main advantages of a VAWT include they are omnidirectional, easy to operate, and the power output can be increased by operating in cluster.

Figure 3 shows different types of wind turbines [13]The Darrieus Vertical Axis Wind Turbine (VAWT) uses lift forces to produce rotational motion and has curved blades that resemble an eggbeater. Savonius Vertical Axis Wind Turbine (VAWT): The Savonius VAWT features an easy-to-understand design with S-shaped blades that are angled vertically to absorb wind energy through drag forces, making it appropriate for low wind speeds. H-type Vertical Axis Wind Turbine (VAWT) uses straight blades mounted to a central vertical axis to efficiently capture wind energy and produce electricity in a variety of wind conditions.[13]
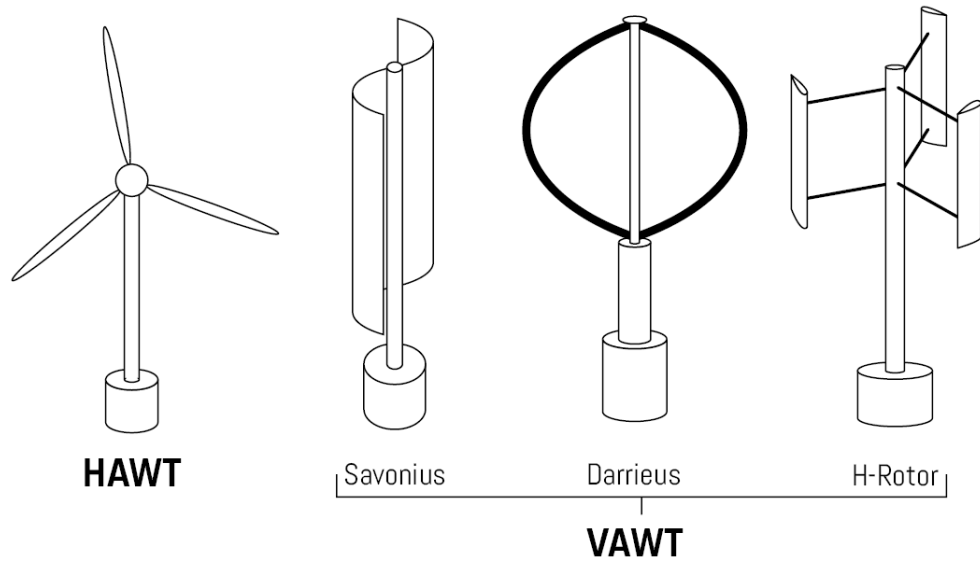
Figure 4: Different types of wind turbines [13]

2.6 VAWT farms

Unlike HAWT, VAWT are found to produce better performance when operated in cluster. HAWT are generally placed at 5-6 times diameter of the rotor. VAWT in cluster produced slightly higher performance when the experiment was conducted in desert [9], but for equal spacing HAWT experienced a 20-50 % lesser efficiency. From this experiment it was clearly proved that VAWT wind turbines perform more when operated in cluster. Figure 4 shows different methods that exist in types of cluster formations used in VAWT.
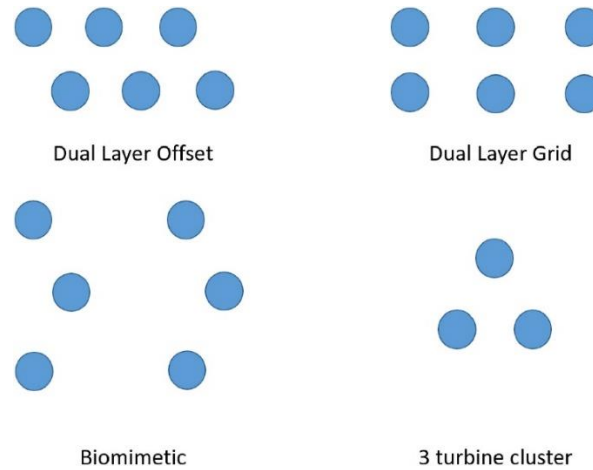
Figure 5: Different configurations of Wind Turbine Farm [12].

2.7 CFD analysis of VAWT

Several studies can be identified which are dealing with the CFD analysis of a Wind Turbine as CFD methods are capable of producing outcomes that are well in line with experimental data.

The Navier-Stokes equations, which are basic in the study of computational fluid dynamics (CFD), are essential for modelling and deciphering the behavior of fluid flows.

The continuity equation and the momentum equation are the two primary equations that make up the Navier-Stokes equations. Let's go in depth about each equation:

First, the Continuity Equation The concept of mass conservation for an incompressible fluid is expressed by the continuity equation. According to this rule, the net rate of mass flow into or out of a control volume is equal to the rate of change of mass inside that volume. The continuity equation is provided by:

$$\nabla \cdot (\rho \, \mathrm{u}) = \qquad\qquad\qquad\qquad\qquad \text{(Eq.1)}$$

Where $\nabla \cdot$ denotes the divergence operator, ρ denotes the fluid density, and u denotes the fluid velocity vector, the equation reads: (u) = 0. This equation guarantees the fluid's incompressibility, which prevents the density from drastically varying across the flow domain.

Secondly, Momentum Equation: The momentum equation explains how fluid motion and the forces acting on it relate to one another. Both the pressure forces and the viscous forces are considered. It is possible to write the momentum equation for an incompressible fluid as

$$\rho \left(\partial u / \partial t + u \cdot \nabla u \right) = -\nabla p + \mu \nabla^2 u \qquad \text{(Eq.2)}$$

where $\partial u / \partial t$ is the rate of change of velocity with respect to time, $u \cdot \nabla u$ denotes the convective acceleration term, p represents pressure, μ denotes dynamic viscosity of the fluid, and Laplacian operator applied to the velocity vector u is denoted as $\nabla^2 u$. [56][57][58]

CFD techniques can be computationally expensive as they require large domains and finer meshes in areas of computational interest. The present study follows the ideas introduced by [10]. The URANS equations with elliptic blending was used in this approach and can be written as follows:

Continuity Equation:

$$\nabla \cdot (\rho u) = 0 \qquad \text{(Eq.3)}$$

Momentum Equations:

$$\partial(\rho u)/\partial t + \nabla \cdot (\rho uu) = -\nabla p + \nabla \cdot (\mu (\nabla u + (\nabla u)^T)) + S \qquad \text{(Eq.4)}$$

Here, ρ is the density, u represents the velocity vector, t is time, p is the pressure, μ is the dynamic viscosity, and S represents the source terms.

The elliptic blending method involves adding an extra elliptic equation to the regular URANS equations. The momentum equations are multiplied with the blending function, which is a fluid transition function between the parabolic and elliptic sectors. This blending function makes sure that the model operates as an elliptic equation in areas of laminar or transitional flow and as a parabolic equation in areas of totally turbulent flow. The added elliptic equation enhances the accuracy of the viscous effects.

The modified momentum equation follows

Momentum Equations:

$$\partial(\rho u)/\partial t + \nabla \cdot (\rho uu) = -\nabla p + \nabla \cdot (\mu (\nabla u + (\nabla u)^T)) + S + B \quad (Eq.5)$$

Elliptic Equation:

$$\nabla \cdot (\alpha \nabla u) = \nabla \cdot (\alpha \nabla B) \quad\quad\quad\quad\quad (Eq.6)$$

In these equations, B stands for the blending function, and α is the blending process control constant. The supplementary elliptic equation that results from the continuity equation and meets the following requirement is solved to get the blending function B:

$$\nabla \cdot (\rho B) = 0 \quad\quad\quad\quad\quad (Eq.7)$$

Particularly in areas where laminar and turbulent flows coexist or quickly

switch from one to the other, one can get more accurate results by solving the modified URANS equations with the elliptic blending approach.[10]

2.8 Aerofoil in VAWT

Aerofoil shapes used in VAWT are of two types a) Asymmetric type and b) Symmetric type. Various studies were conducted to find which aerofoil shape yields more power coefficient. For a given application, the choice of an asymmetric or symmetric aerofoil is influenced by several variables, such as the required performance characteristics, operating circumstances, and design criteria. Although asymmetric aerofoils can be more efficient at low tip speed ratios, the best configuration to use will depend on the design and operating circumstances. When building VAWTs with high tip speeds, symmetric airfoil shapes like the NACA 0012, NACA 0015, NACA0018 or S-series airfoils are frequently used. In applications where the blades may experience changing wind conditions and rotating speeds, these airfoils have the benefit of offering equal lift characteristics at positive and negative angles of attack. The precise size of the efficiency gain might change based on the particular design and operating circumstances. When comparing various aerofoil shapes and found that for an H type rotor NACA0018 produced more power coefficient [39][40]. The previous researchers from the same lab, [10] conducted studies on NACA0018. Due to these reasons a symmetric type NACA0018 is selected for conducting CFD analysis.

The number of blades in a turbine is another important criterion, which was studied by numerous researchers to improve the efficiency of a vertical axis wind turbine. Commonly used turbines consist of three blades or four blades. It was found that for lower loads, both three bladed turbines and four bladed turbines show similar efficiency, whereas for higher loads three bladed turbines have slightly higher efficiency There are several reasons why three-bladed turbines often operate more efficiently

than four-bladed turbines at greater loads.

1. Aerodynamic Performance: Three-bladed turbines frequently have better aerodynamic profiles, allowing them to effectively capture more wind energy. The blades' airfoil shape and angle of attack were meticulously tuned to maximise the amount of energy captured from the wind. The efficiency of the design may be improved, especially at greater loads when the turbine is working closely to its full capacity.

2. Structural considerations: As the number of blades increases, the turbine's construction becomes more complicated, and the rotor hub and blades are subjected to more loads and stresses. Increased weight and associated structural issues may result from this. Three-bladed turbines, on the other hand, benefit from a more straightforward design that is balanced and can tolerate greater loads more successfully, leading to enhanced efficiency under greater loads.

3. Wake Effects: Downwind of a wind turbine, there are wakes, which are regions of reduced wind speed and more turbulence. The performance of nearby wind farm turbines may be hampered by these wakes. In a four-bladed turbine, the addition of additional blades can lead to increased wake interactions and efficiency losses. Three-bladed turbines, which have fewer blades, typically produce wakes that are simpler to manage and less complicated, retaining greater efficiency at higher loads. [38][41]

2.9 VAWT in farm configuration

Performance of pairs of vertical axis wind turbines was also studied by a number of researchers, but vertical axis wind turbines with multiple turbines under farm configuration was yet to be explored. Pairs of Vertical Axis Wind Turbine (co-rotating, counter-rotating) were reviewed, and the counter-rotating (up type) produced the best power coefficient in pairs.

Studies were conducted on pairs of vertical axis wind turbines, at different combinations of array angle, distance between turbine and direction of rotation [15] Hansen et.al. It was found that at an array angle of 60 degrees, the performance of a pair of vertical axis wind turbines improved by 15%.

2.10 Summary

Finding the best layout for VAWT, which is the project under consideration, was identified to be feasible and capable of being a part of scientific study on wind energy. Including more rotors in the layout can help this study to be more compatible for wind farms and not a lot of studies have been done in this area. So there exists a research gap that this study can fill. VAWTs in farm configuration is an area of great research interest as they have been proved to enhance efficiency when used in cluster. CFD simulations must be set up adapting the best methodology available, reducing the computational time and without reducing the accuracy.

3. Methodology

Numerical study is completed using steps illustrated on flowchart in Fig.5 for every chosen simulation. The methodology for conducting the CFD analysis is broadly classified into preprocessing, Processing and post processing. Pre-processing involves selection of geometry and generation of mesh. NACA 0018 blade was identified to be the best aerofoil geometry to get optimized results, from similar research in the same field. The generation of geometry (modelling) was done in CAD, SOLIDWORKS software is used in this particular analysis. Different meshing techniques are adopted as one of the main objectives of the study is to reduce the computational time. Structured, Polyhedral and tetrahedral mesh were used in a single rotor system and polyhedral mesh was identified to be producing the best result in minimum computational time, the same was used for the analysis of two rotor, three rotor, four rotor and five rotor systems.

This assertion was based on the results of a specific research or analysis, polyhedral mesh delivered the best outcome with the least amount of computing work. Researchers frequently consider a number of variables while comparing alternative meshes, including accuracy, computational effectiveness, convergence behavior, and overall solution quality. These elements, in addition to the unique needs of the research, are probably what led to the polyhedral mesh being chosen as the top performance. Regarding the justification for various mesh types, various meshes might in fact create a variety of outputs because of their traits. For example, the strengths and

drawbacks of hexahedral, tetrahedral, and polyhedral meshes vary. Tetrahedral meshes are more versatile but may need a larger cell count to attain accuracy, whereas hexahedral meshes are noted for their precision and efficiency in capturing complicated shapes. In many situations, polyhedral meshes are a desirable option because they strike a good compromise between accuracy and computational efficiency. For realistic simulations, a y+ value of around 1 at places of computational importance.
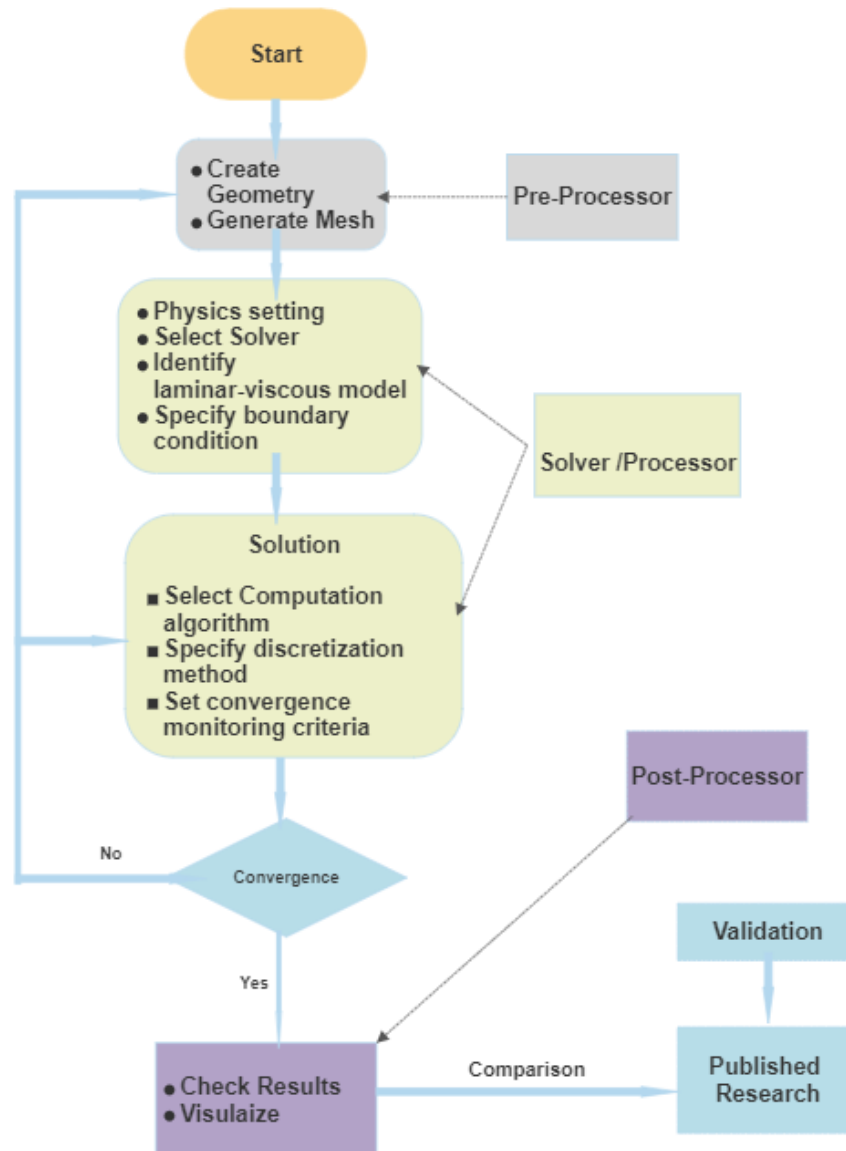

Figure 6: Flow chart showing the methodology undertaken.[45]

It guarantees that the initial cell near to the wall is situated inside the viscous sublayer of the boundary layer when y+ is close to 1. This is crucial because the viscous sublayer is where the flow characteristic such as velocity gradients and shear stress are most essential. The meshing method successfully captures the velocity gradients by keeping the near-wall cells small and maintaining a y+ value close to 1, leading to superior predictions of the boundary layer behavior. [46][47].

Processing involves physics setting, selection of solver, identifying the model and setting up the boundary conditions. These steps are discussed in detail in the following sections. It was found from recent research [10] using Star CCM+ in similar fields that the Reynolds stress turbulence model has many advantages over the others, it's more accurate and compatible with the current study. Transient, segregated algorithms were used for the study referring to previous research in computational fluid dynamical analysis of turbines.

If the convergence study is found to be producing positive results, the next step would be to check and visualize the results. The moment coefficients were plotted, the scalar and vector plots of velocity were visualized. The results were then validated using.

The following steps were performed, for the 3D analysis, the same steps can be followed for a 2D analysis also, expect for the fact that the 3D is converted to 2D in Star CCM+, after meshing. Table 2 shows the difference between different aspects (dimensions, boundary conditions, outcomes) for 2D and 3D analysis.

A 3D model is made using solid works which is 12 meters of blade height.

This is imported into Star CCM+. The geometry consists of three rotor blades and the central cylindrical pole of the turbine. A cylindrical rotating sub domain is created over the rotor blades using a new shape part option in Star CCM+. This means rotating cylindrical subdomain is created around the rotor blades. This indicates the definition of a cylindrical area close to the blades, precisely aligned with the turbine's rotating axis. This subdomain was developed to examine and research the flow dynamics and features present in this area. The length of the blade is given as 12 m, the length of the central pole is 16m and the other dimensions are similar to the 2D analysis. The blades are contained inside the rotating domain. The radius of the cylindrical domain is set as 15 m to contain the rotor fully inside, and the length is set as 12m which is same as that of the blade length. The stationary domain is also created using the new shape part option. The stationary domain is a rectangular block, the cylindrical rotating sub domain is contained inside the stationary domain. The length of the rectangular stationary domain is given as 14 D and the breadth is given as 10 D, where D is the diameter of the rotor.

Subtract operation is performed to separate the rotation fluid domain and the stationary fluid domain. Using the Boolean subtract operation in Star CCM+, the blades and the pole are subtracted from the cylinder this forms the cylindrical rotating fluid domain. The whole cylinder with the blades and the central pole is then subtracted from the rectangular block, which forms the stationary fluid domain.

The parts are created, now the regions must be assigned using the assign parts to regions option in Star CCM+, The regions are assigned to the virtual rotating sub domain (the one which is made using subtract option in the previous step) and the stationary wind tunnel.

The interface is defined between the two domains (rotating domain and

stationary domain) using the create interface option. Mesh is created using mesh continua option, the base size is set to 8m. Volume controls were also provided for the rotating parts as they are parts of computational interest. Two volume controls were defined, one for the cylindrical rotating sub domain and the other for the blades. Prism layers were also provided near the walls of the blade to get accurate results.

Volume controls are provided for the cylindrical rotating subdomain and near the vicinity of the blades. The number of prism layers are set to be 20, the thickness for the prism layers is set to be 0.05 and a prism layer stretching value was set as 1.5, surface growth rate of 1.3 was given and the minimum target size is set as the same as that of the base size.

Boundary conditions is same as that of the 2D analysis. (Figure 10, Table 2) An implicit, unsteady, segregated, constant density, turbulent flow under the Reynolds stress turbulence model with elliptic blending is selected under physics continua. Rotation is assigned to the rotating domain using the motion rotation option form tools in Star CCM+. To assign this rotation to the rotating region, motion specification under the virtual rotating subdomain is given as rotation.

Table 2: The difference between different aspects (dimensions, boundary conditions, outcomes) for 2D and 3D analysis

Comparison Aspect	2D Simulation	3D Simulation
Velocity	10 m/s	10 m/s
Reference Pressure	101,325 Pa	101,325 Pa
Length of the Domain	14 D	14 D
Breadth of the Domain	10 D	10 D
Height of the Domain	NA	16 m
Air Density	1.18415 kg/m	1.18415 kg/m
Dynamic Viscosity	1.85508 · 10-5 kg/(m s)	1.85508 · 10-5 kg/(m s)
Aerofoil	NACA0018	NACA0018
Turbine Diameter	20 m	20 m
Chord	1 m	1 m
Turbine height	NA	12 m
Blade end- fillet radius	0.01 m	0.01 m
Wall Boundary Conditions	Symmetry planes for side walls and interface between stationary and rotating domain.	Symmetry planes for side walls, top, bottom wall and interface between stationary and rotating domain.
Inlet Boundary Conditions	Velocity inlet, 10 m/s	Velocity inlet, 10 m/s
Outlet Boundary Conditions	Pressure outlet ,1 atm	Pressure outlet ,1 atm
Moment Coefficient	0.137	1.632

3.1 Computational Domain and regions

Flow chart shows the different steps in the methodology undertaken. Initially a turbine in isolation is made and then the number of rotors can be increased to make it closer to the farm field situation. The first step was to make the rotor geometry in CAD. Dimensions for the rotor design is found from previous literatures as shown in Figure 9. STAR CCM+ was identified to be the most suitable software for the current study and was successful for much research of similar parameters. This was then exported to STAR CCM+, the rotor geometry was made similar to [15] Hansen et.al. so that this can be validated. The vertical height of the blade was given a 2m length while making the CAD model, which can be later converted to for 2D analysis. The vertical height of the blade is the distance, measured perpendicular to the ground from the base to the highest point of the blade. This is used to make the 3D model which is in turn converted to 2D after meshing. The chord of a blade is the length of the blade divided by the straight-line distance between the leading edge and the trailing edge. It displays the breadth of the blade along the whole length of its span. Chord length is 1 m. Table:3 shows different geometric parameters of the VAWT rotor used to conduct the study.

Table:3 Geometric parameters of the VAWT rotor used to conduct the study

Name	Symbol	Value
Aerofoil		NACA 0018
Turbine diameter	D	20 m
Chord	c	1 m
Blade end - fillet radius	r	0.01 m

After exporting the CAD model computational domains were defined. Cylindrical routing sub domain and a stationary rectangular domain is

defined. After performing the subtract operations (subtract operations and definition of interface are important as we have a sliding contact between the two regions). For assigning the rotation to the cylindrical rotating sub domain the tool motion rotation is used and a rotation is specified for the cylindrical domain. An angular velocity of 3.5 rad/s is given to the cylindrical rotating sub domain about the Z axis. Figure 6 shows the computational domain for the CFD analysis of VAWT.D represents the diameter of the rotor as given in Table 3. Table 4 shows different flow parameters of the VAWT rotor used to conduct the study.
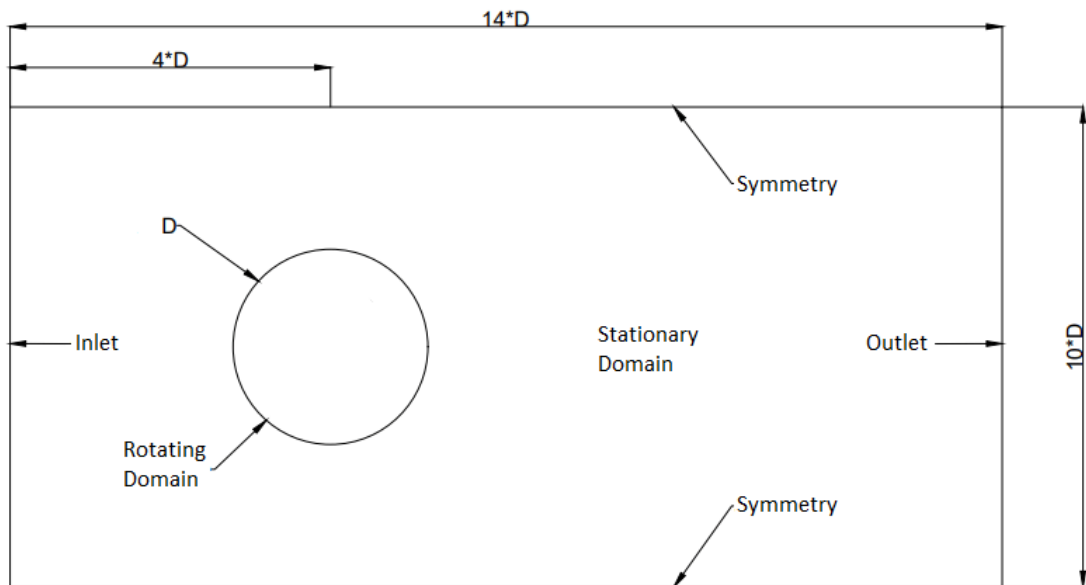
Figure 7: Computational domain for the CFD analysis of VAWT.D represents the diameter of the rotor as given in Table 3.

Table 4: Flow parameters of the VAWT rotor used to conduct the study

Flow Parameter	Description
Velocity	10 m/s

Reference Pressure	101,325 Pa
Reynolds number – blades Re_b	Minimum: $1.69 \cdot 10^6$ Maximum: $3.04 \cdot 10^6$
Reynolds number – turbine diameter	Re $1.35 \cdot 10^7$
Air Density	1.18415 kg/m
Dynamic Viscosity	$1.85508 \cdot 10\text{-}5$ kg/ (m s)
Wall Boundary Conditions	Symmetry planes for side walls and interface between stationary and rotating domain.
Inlet Boundary Conditions	Velocity inlet, 10 m/s
Outlet Boundary Conditions	Pressure outlet ,1 atm

3.2 Bounmdary conditions
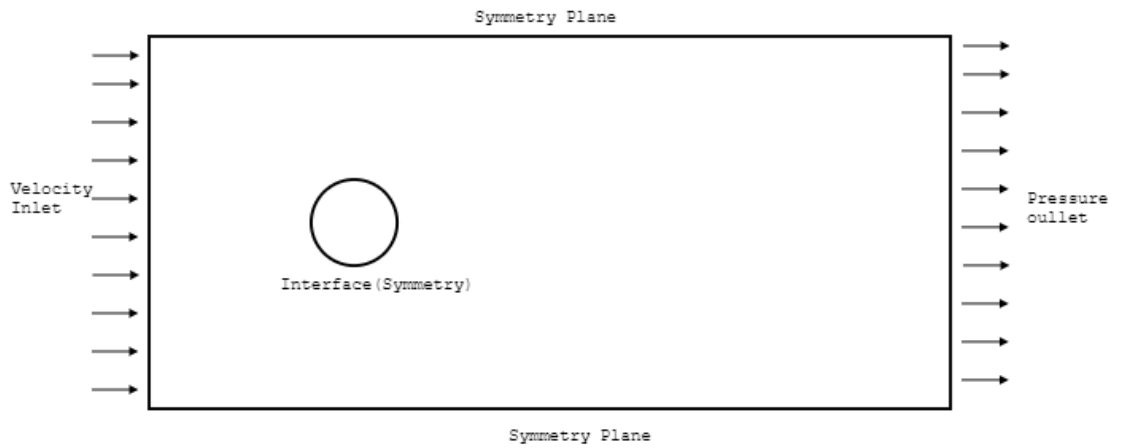
Figure 8: Figure showing the boundary conditions used.

Table 5: Various boundary conditions used to conduct the study.

Condition	Settings
Inlet	Velocity inlet with a velocity of 10 m/s. Turbulent Intensity
Outlet	Pressure outlet with a gauge pressure of 0 Pa as there is no forced pressure differential across the system.
Walls	The blades were modelled as rigid bodies as the Fluid-Structural interactions would be insignificant.
Domain	Air at default settings (Sea Level).
Symmetry	Applied to side walls and interface

Figure 6 shows the boundary conditions used. Table 5: Various boundary conditions used to conduct the study. A model was developed with cylindrical rotor rotating inside a stationary rectangular domain. As shown in the figure the velocity inlet is defined with 10 m/s and pressure outlet with 0 Pa. Side walls and interfaces were modelled as symmetrical plane. The walls of the blades are defined as rigid bodies. Reynolds number for the conducted at a turbine diameter Reynolds number of $1.35 \cdot 10^7$ The tests by Brownstein, Wei, and Dabiri were carried out at a Reynolds number that was 185 times lower than the one used in this study. A pair of VAWTs were put through wind tunnel experiments by Brownstein, Wei, and Dabiri (2019) at a Reynolds number of $7.3 . 10^4$ The scaled model would have to be very small to minimize blockage effects, which further complicated obtaining reliable data. The Reynolds number would never correspond with the CFD models. To ensure there were no gaps, it was decided to devote all the time and attention to the CFD model.

3.3 Meshing

Different types of meshes like polyhedral, structured and tetrahedral mesh were applied to the domain initially (Figure 7), later it was found that all the meshes will produce similar results with respect to monitors, plots and scalar scenes. Eventually polyhedral mesh was selected for performing further analysis and studies as the gradients will be well approximated, since each cell has the greatest number of neighboring cells when compared with other two types of meshing techniques. It was also identified from literature that polyhedrons are least sensitive to stretching when compared to tetrahedral and structured meshes, which will eventually result in better quality of mesh, this might in turn lead to better numerical stability. From the mesh convergence study the base size was fixed to be 8m or less.
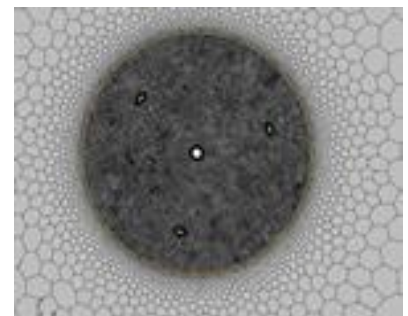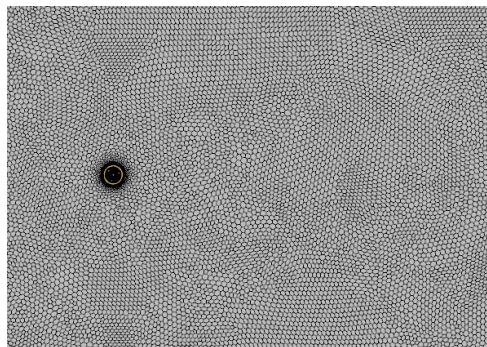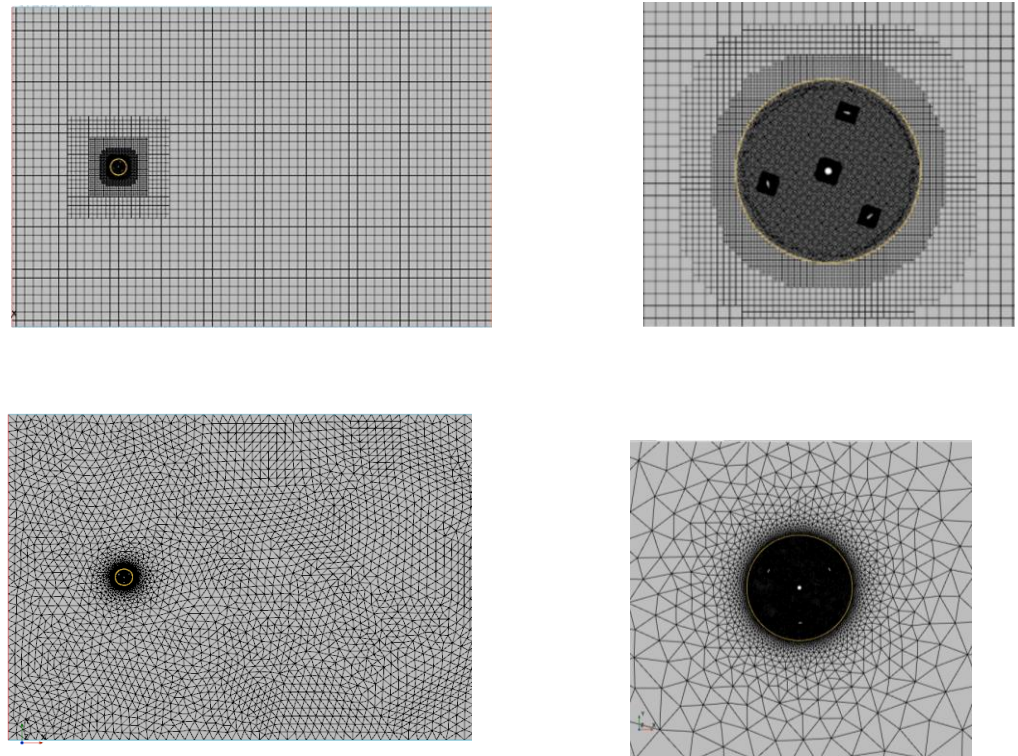
Figure 9: Different types of meshing techniques adapted.

To find the percentage error the following method was used. The moment coefficients from the tetrahedral mesh and the polyhedral mesh are Cm_tetra(0.135) and Cm_poly(0.137), Cm_struct(0.136) structured mesh respectively, reference moment coefficient is taken Cm_reference (0.137)obtained from Hanse et.al [15]

Absolute differences: |Cm_tetra - Cm_reference|, |Cm_poly - Cm_reference| |Cm_struct - Cm_reference| was found out.

Use the following formula to get the percentage inaccuracy for each mesh type:

(Absolute difference / Reference solution) * 100 = Percentage mistake

For instance, the tetrahedral mesh error % would be: Tetrahedral mesh error percentage is (|Cm_tetra - Cm_reference| / Cm_reference) * 100.

The percentage of error was found to be less than 2% for all the cases.

This assertion about polyhedral mesh was also based on the results of a specific research or analysis polyhedral mesh delivered the best outcome with the least amount of computing work. Researchers frequently consider a number of variables while comparing alternative meshes, including accuracy, computational effectiveness, convergence behavior, and overall solution quality. These elements, in addition to the unique needs of the research, are probably what led to the polyhedral mesh being chosen as the top performance. Regarding the justification for various mesh types, various meshes might in fact create a variety of outputs because of their traits. For example, the strengths and drawbacks of hexahedral, tetrahedral, and polyhedral meshes vary. Tetrahedral meshes are more versatile but may need a larger cell count to attain accuracy, whereas hexahedral meshes are noted for their precision and efficiency in capturing complicated shapes. In many situations, polyhedral meshes are a desirable option because they strike a good compromise between accuracy and computational efficiency. For realistic simulations, a y+ value of around 1 at places of computational importance. It guarantees that the initial cell near to the wall is situated inside the viscous sublayer of the boundary layer when y+ is close to 1. This is crucial because the viscous sublayer is where the flow characteristic such as velocity gradients and shear stress are most essential. The meshing method successfully captures the velocity gradients by keeping the near-wall cells small and maintaining a y+ value close to 1, leading to superior predictions of the boundary layer behavior. Volume controls were also provided for the rotating parts as they are parts of computational interest. Two volume controls were defined, one for the cylindrical rotating sub domain and other for the blades. Prism layers were also provided near the walls of the blade to get accurate results.[46][47]

Volume controls are provided for the cylindrical rotating subdomain and near the vicinity of the blades. The number of prism layers are set to be 20, the thickness for the prism layers is set to be 0.05 and a prism layer stretching value was set as 1.5, surface growth rate of 1.3 was given and the minimum target size is set as the same as that of the base size.
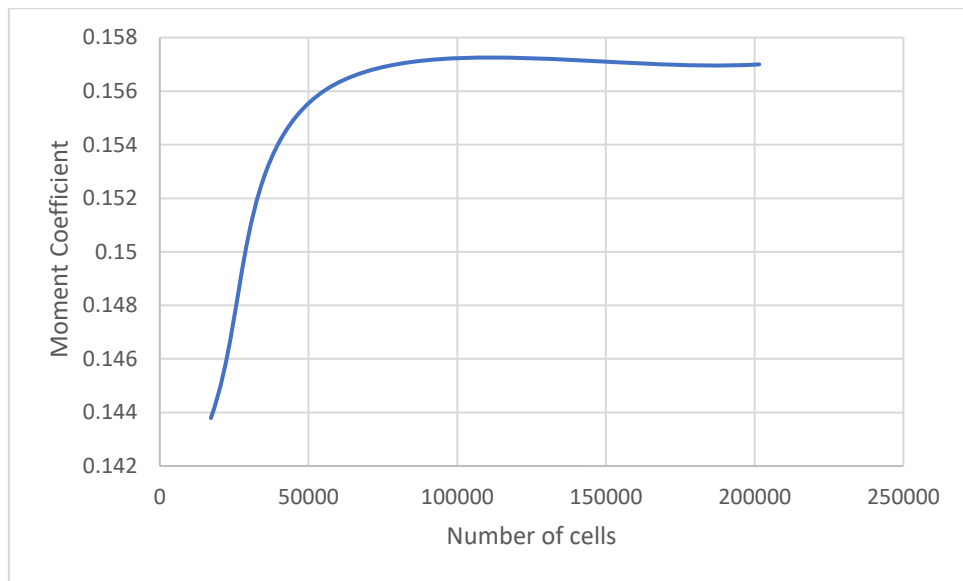
3.4 Mesh Convergence study

Figure 10: Graph showing moment coefficient value for different number of cells for a single rotor system.
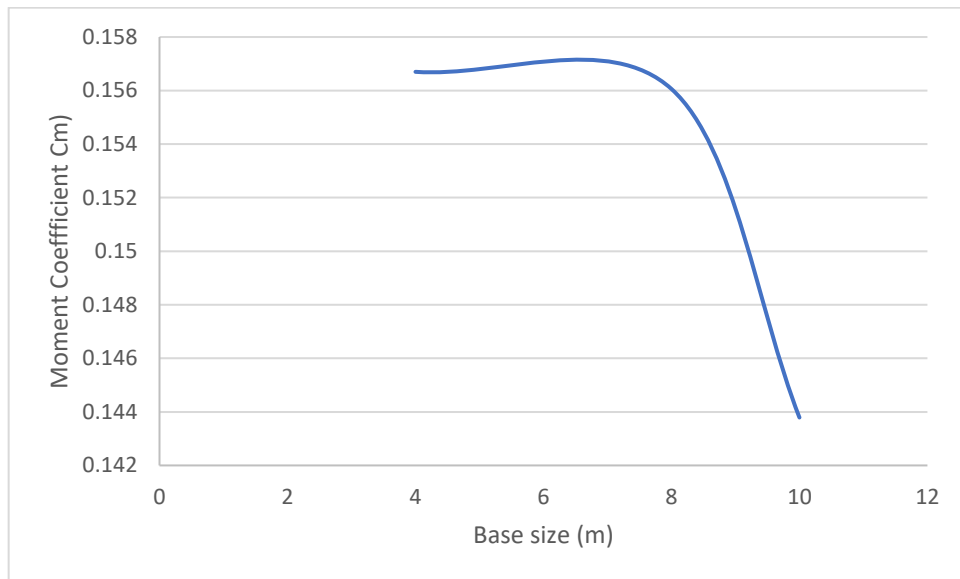
Figure 11: Graph showing moment coefficient value for different base sizes for a single rotor system.

The simulation might have slightly different outputs for different mesh size and number of meshes. It is a usual practice to conduct the mesh convergence study for such cases. The most important parameter under study was Moment coefficient. Figure 8 shows the variation in moment coefficient by increasing the number of cells. Figure 9 shows the variation in moment coefficient at different sizes of the mesh. For analyzing the performance of the simulation under different meshing for the domain as study was conducted in which the number of cells were increased progressively, it was found that when the number of cells reaches 100000, if the number of cells is increased the moment coefficient tend to be constant. Which showed that the meshing is suitable for the analysis. Mesh convergence study is also tested for different base sizes, it was found that for base size of 8 m and below the moment coefficient tend to be constant.

3.5 Definition of Physics

A Two-Dimensional flow analysis was preferred over Three-dimensional analysis, as it reduces the computational time and considering the symmetry of the VAWT to be analyzed. The transient method was selected for the study since it was found to be more numerically stable. Segregated flow algorithm was used over coupled flow as it generates almost the same results referring to previous studies but reduces the memory usage by half. Velocity and pressure components are solved for small increments and in a sequential manner.

Almost all studies in similar flow analysis uses an incompressible flow of air (constant density) since the flow considered has very low Mach number incompressible flow can be assumed as the effects are minimal. [10] recommends the usage of Reynold stress turbulence model for wind turbines as it was found from recent research [10] using Star CCM+ to produce stable results for rotating domains. Th k-ω SST models were also identified to be feasible for the current study and was used by many researchers in the same field, but Reynolds stress turbulence with elliptic blending was preferred over the k-ω model considering the results from recent papers [10] in flow analysis.

3.6 Array of VAWTs

As mentioned earlier the methodology was supposed to be a applied to larger wind farms having more number of rotors, so it will be more realistic to use an array of wind turbines instead of single or dipoles as shown in Figure 10. VAWTs are found to perform much better in clusters rather than in an isolated situation. To find out the efficiency

46

of a VAWT in cluster the power produced by an individual VAWT in isolation is found and compared with that of an array. The ratio of power produced by the cluster of wind turbine to the power produced by the individual wind turbine divided by the number of rotors in the cluster will give the performance indicator of the cluster. For finding out the efficiency of VAWT, monitors are set in STAR CCM+ to identify the moment coefficient of the rotor blades.
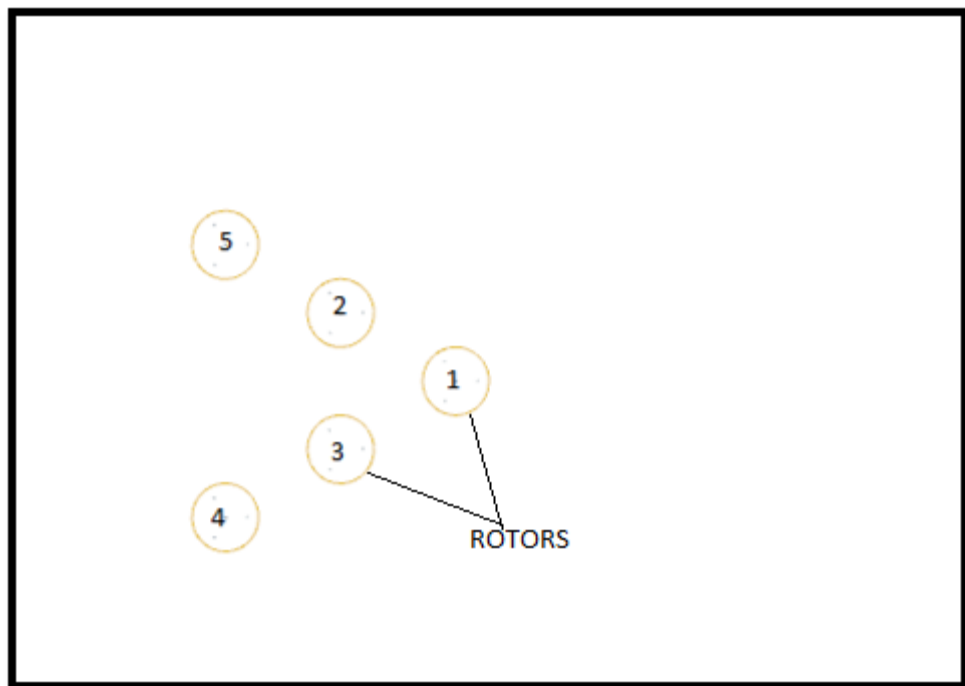

Figure 12: Example of a VAWT array system under study.

Moment Coefficient: Moment coefficients are used in wind engineering to measure the moment (or torque) produced by a body or structure as a result of wind forces. Moment coefficients are derived by dividing the moment experienced by the body or structure by a reference value (such as dynamic pressure or velocity) and are frequently represented by the sign "Cm".[48][49]

Moment coefficient: Cm = M / (0.5 ρ AV^2)

(Eq.8)

Where: Moment coefficient = Cm M = The body's or structure's moment or torque ρ = the air density A = Area of reference V = Wind speed

The efficiency of a turbine or the aerodynamic performance of a body or structure in producing rotating forces in response to wind may be measured by the moment coefficient, which is a dimensionless number. After finding out the moment coefficient against the physical time graph of a VAWT the average value of moment coefficient can be found out by exporting the data points to a csv file. After that power coefficient(C_p) was found using equation 2, where R represents radius of the rotor, R= 10 m, ω is the angular speed in radians per second ω=3.5rad/s, and the free stream velocity, U_0=10m/s.

$$C_p = C_m \cdot \lambda = C_m \cdot R \cdot \omega/U_0$$

(Eq.9)   After finding the value of C$_p$, performance coefficient(Ω) can be found out from the equation 3. Where C_{p_iso} is the power coefficient in isolation.

Performance Indicator of an array of wind turbines = (Power Produced by the array of Wind Turbines) / (Power Produced by Individual Wind Turbine * Number of Rotors in the array)

The performance indicator of a wind turbine cluster is calculated by dividing the total power produced by the entire cluster of wind turbines by the total power produced by a single wind turbine multiplied by the number of rotors in the cluster. The reason for this relationship is that the size and effectiveness of the rotor closely correlate with the amount of power produced by a wind turbine. The combined power generated by a cluster of wind turbines relies on the power provided by each

turbine separately as well as the number of turbines in the cluster.[50]

$$\Omega = \frac{\sum_{i=1}^{n} C_{pi}}{n \cdot C_{p-iso}} \qquad \text{(Eq.10)}$$

If the value of the power coefficient (Ω) is above unity, it can be inferred that the configuration has increased the efficiency and if it is below unity, the efficiency has decreased. To get the efficiency in percentage subtract unity from the Ω value and multiply it by 100. For example, if the Ω value is 1.22 the increase in efficiency due to the configuration of array is 22%.

3.7 Validation

Validation of the CFD simulation was done by simulating a rotor in isolation and its blade Moment coefficient against Azimuth angle plot was compared to the results of [15] Hansen et.al. This particular study is chosen for 15dimensions for the rotor, and the aero foil being NACA0018. The difference in methodologies is that [15] Hansen et.al used an Overset mesh approach whereas this set up uses a sliding mesh approach. The top and bottom boundaries were defined as walls by [15] Hansen et.al. while they are defined as symmetry planes in the current study, so that area of the stationary region can be reduced. The area of the stationary plane was 0.25 times that of the previous study.

The correlation confirmed that the CFD model was well in line with the study conducted with [15] Hansen et.al. The CPU hours for simulating 17 complete revolutions (approximately 30 seconds of flow time) of the rotor was 91 hours for [15] Hansen et.al was 9.5 hours for the proposed methodology (11th Gen Intel(R) Core (TM) i9-11900K @ 3.50GHz, 3504 Mhz, 8 Core, 16 Logical Processor). The CPU hours

were reduced by 90%. It can be concluded that the current study reduces the computational time to a great extent without compromising on the accuracy. This makes the proposed methodology c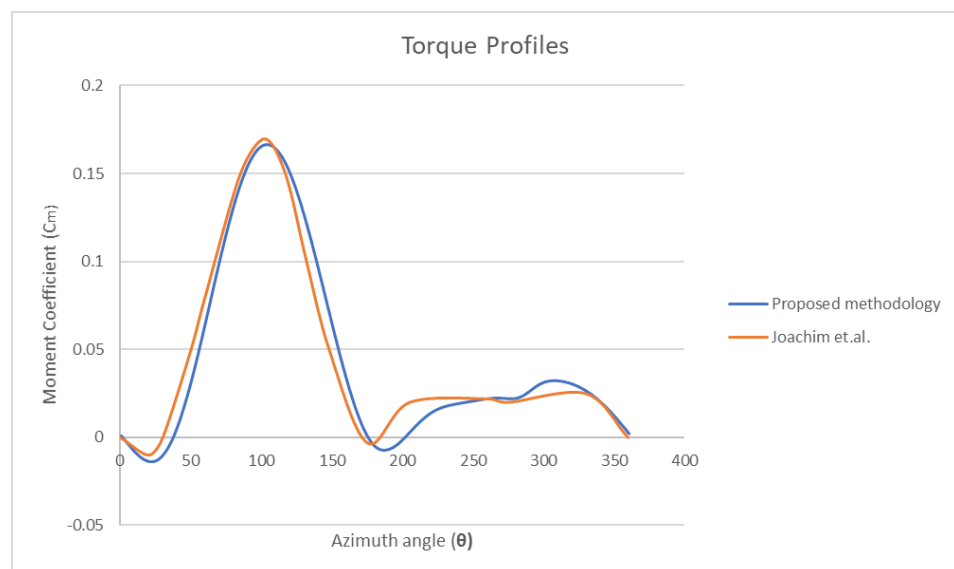omputationally inexpensive and faster compared to the earlier one. The torque profile of a rotor blade, where the rotor was in isolation over an Azimuth angle of 0 to 360 degree super imposed over the torque profile of the same explained by [15] Hansen et.al as shown in Figure 11. It shows that the findings from the two techniques are comparable, which is a crucial confirmation of the precision and dependability of the torque profile of the rotor blade. the azimuth angle (which ranges from 0 to 360 degrees) plotted on the x-axis and the torque values on the y-axis when superimposing the torque profiles. The validation graph shows that, with only slight variations, the findings from both techniques are equivalent. This validation backs up both methodologies' accuracy and encourages the application of the proposed methodology for further studies.

Figure 13: Torque profile of a rotor blade, where the rotor was in isolation over an Azimuth angle of 0 to 360 degree super imposed over the torque profile of the same

explained by [15] Hansen et.al.

Sliding Mesh (SM) and Overset Mesh (OM)

Meshing is a compulsory part of conducting CFD analysis, however for studies that contain a rotating domain the two types of meshing usually adapted are Sliding mesh and Overset mesh. In sliding mesh technique there will be a rotating domain and stationary domain, the rotating domain slides pass the stationary domain. Where as in overset mesh the rotating domain overlaps the stationary domain.

Flow pattern of a Vertical Axis Wind Turbine is found to be unsteady in and around the vicinity of the blades. The reason for the turbulence is

1) Pressure gradient created by the motion of the blades (flow deflection)

2) Pressure wave and freestream interact with each other. [42][43][44]. The impact of the passing blades on the surrounding air is referred to as the interaction between a pressure wave and a freestream. The advancing side of a VAWT, where the blade is going against the wind, and the retreating side, where the blade is flowing with the wind, experience different pressures as the blades revolve. A pressure wave is the term used to describe the pattern of alternating high- and low-pressure areas that is created by this pressure differential. The performance and behavior of the wind turbine are impacted by the pressure wave's interaction with the entering freestream of air. Various factors, including the aerodynamic pressures on the blades, the power output, and the overall efficiency of the VAWT.

3) Interaction of wake and pressure wave with downstream rotor blades.

Many experimental investigations were conducted to identify the flow

unsteadiness of Vertical Axis Wind Turbines. Analytical models were also developed by researchers to capture the unsteadiness of flow of Vertical Axis Wind Turbines. To understand the precise aerodynamic coefficient was not an easy task. This was the major disadvantage in these models.

The aerodynamic behavior of Vertical Axis Wind Turbines can be accurately predicted with CFD models. The accuracy of the CFD analysis depends on the boundary conditions, proper meshing strategy and turbulence modelling.

Sliding mesh and overset mesh are two grinding strategies adopted by most of the researchers for CFD analysis of VAWT.

In both the sliding mesh and Overset mesh approach there are two domains: a stationary domain and a rotating sub domain. Both the domains have relative motion between them, and they are meshed accordingly.

Meshes do not overlap in sliding mesh, but they slide against each other at the interface of the two domains (stationary domain and rotating domain) . Meshes have relative motion with each other according to the time step given, the angular distance covered can be defined in the solver. At each time step the governing equation is solved in the stationary domain and the rotating domain. There should be interchange of information along the interface between the meshes, for that the fluxes across the interface should be estimated. In overset mesh, meshes are generated independently and one overlaps over the other. In this technique there should be background mesh (stationary domain) and near mesh (rotating domain), one or more near meshes can be included over a background mesh. The overlapping region is known as the overset boundary, the governing equation is solved on the overset boundary as well as the meshes (background mesh and near mesh). For obtaining the exact boundary conditions the solution is

iterated and interchanged between the meshes. Mesh generation is less complicated in overset mesh compared to sliding mesh, the number of cells generated also gets reduced as the meshes are created independently. But the main disadvantage is that the size of the element's size of the cells must be compatible with each other on the overset boundary.

To sum up, in both sliding mesh and overset mesh, the meshes from both the domains must merge with each other in order to start the simulation, although the meshes are created independently.

Figure 6 shows sliding mesh and overset mesh technique the dissimilarities between sliding mesh and overset mesh can be summarized as below

> Meshes do not overlap in sliding mesh whereas the overlapping of the meshes in the two domains happen in overset mesh.

> A definite interface is created between the two domains in a sliding mesh technique to obtain information interchange whereas an overset boundary is created in an overset mesh for the same.

> At every timestep, over the overset boundary (overlapping region) the solution must be interpolated.
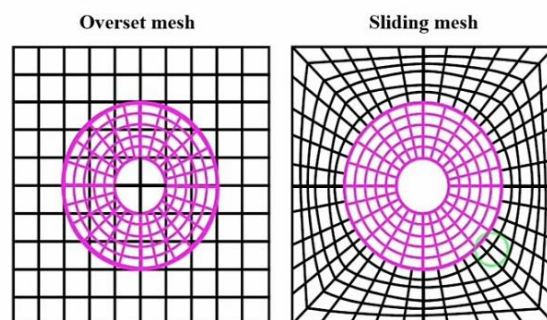
Figure 14: Figure showing sliding mesh and overset mesh technique [11]

4. Results

In this section the various outcomes produced are presented, discussed and analyzed. The velocity contours, vorticity plots, moment coefficient produced by the rotors in various farm configurations are considered.

4 .1 Rotor in isolation

Firstly, a rotor under isolation is considered for analysis.
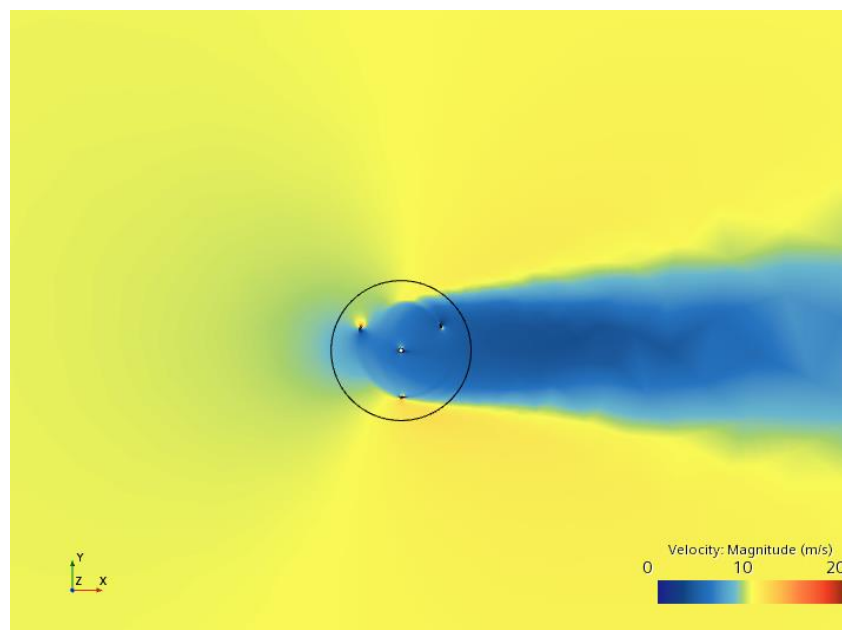
Figure 16: Figure shows the Velocity profile of the configuration under consideration.
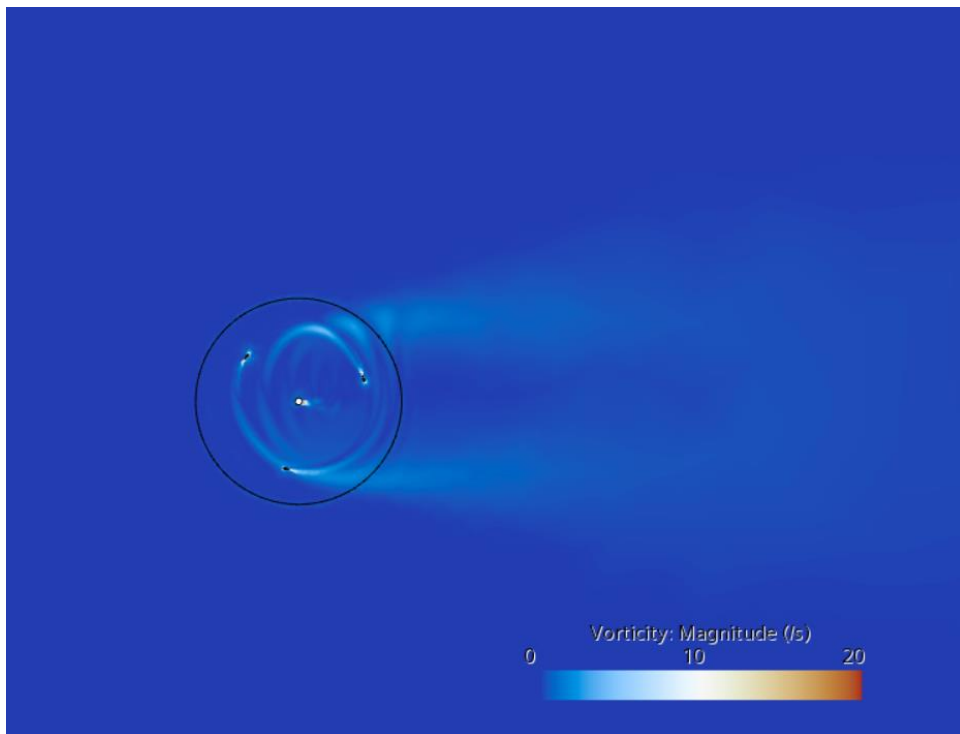
Figure 17: Figure shows the Vorticity profile of the configuration under consideration
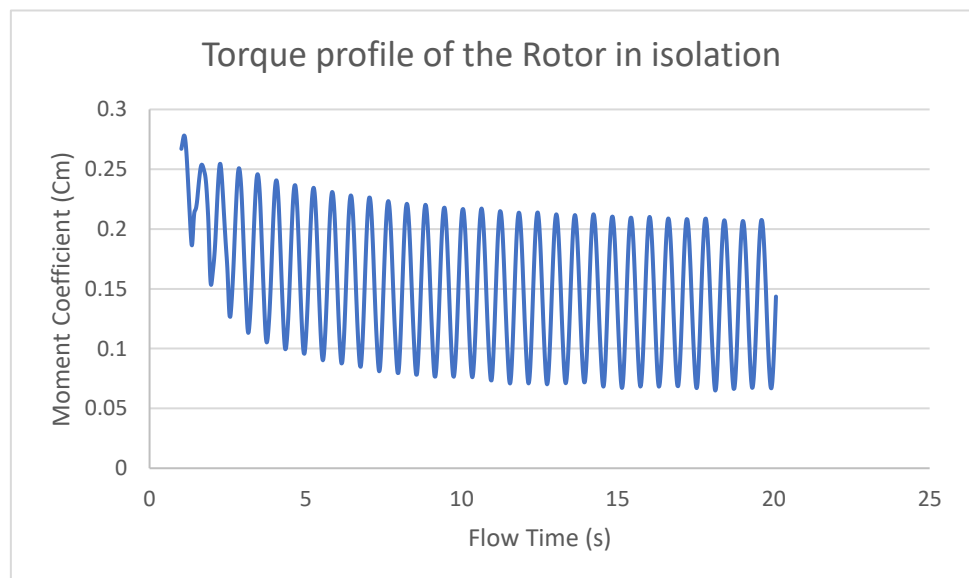
Figure 18: Torque profile experienced by the rotor over the flow time. The position of rotor can be identified from figure 16.

Figure 16 shows the velocity profile of a rotor in isolation. Figure 17 shows the Vorticity profile of the configuration under consideration A single rotor system needs to be simulated before going into different complex configurations. The moment coefficient against flow time graph was also plotted as shown in Figure 18. The purpose of creating a rotor in isolation was to validate the results with that of [15] Hansen et.al. The results have shown that the torque profile of both the cases are matching (explained in the validation section). The performance indicator of a single rotor system will be 1 as there is only rotor in the system. From the torque profile it was found that the Moment Coefficient oscillates between 0.06- 0.25. The average value of moment coefficient being 0.13, which is used to compare the performance indicator of the rest of the configurations. The average moment Coefficient value is 0.137 and the average power coefficient is 0.479, these values are used as a benchmark to find out the performance indicator of other turbines.

The 3D CFD simulation of the vertical axis wind turbine under isolation is also performed using Star CCM+. The dimensions, boundary conditions, outcomes for 3D analysis can be found from Table 2 and the dimensions and details of the domain under study can be found from Figure 6

Figure 19 shows the Velocity profile of the 3D configuration under consideration; the figure is obtained from the transparent view under Star CCM+. the rotating and stationary domain be clearly seen. Figure 20: shows the Velocity profile of (sectional view) of the 3D configuration. The cross-sectional view of the velocity profile is similar to 2D velocity profile. Figure 21 shows torque profile experienced by the rotor (3D) over the flow time, as we can see the moment coefficient

has increased proportionally compared with Figure 18.
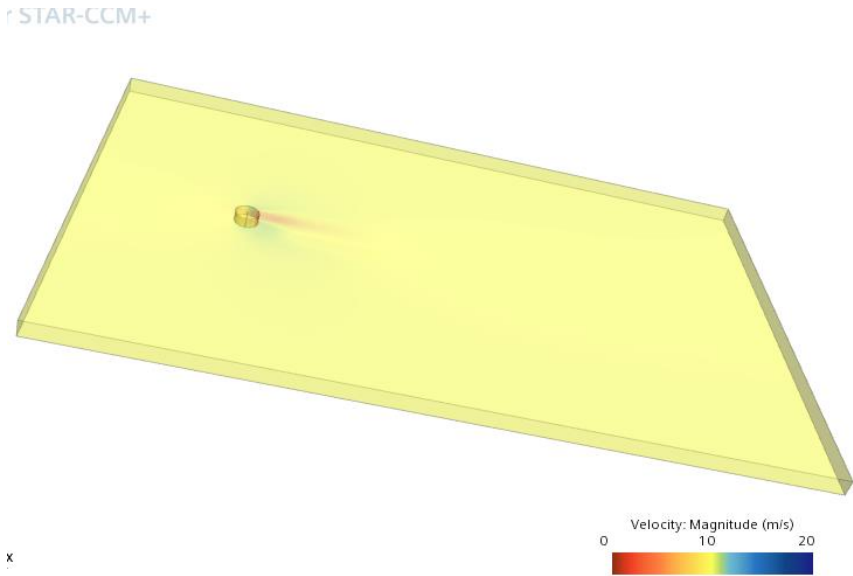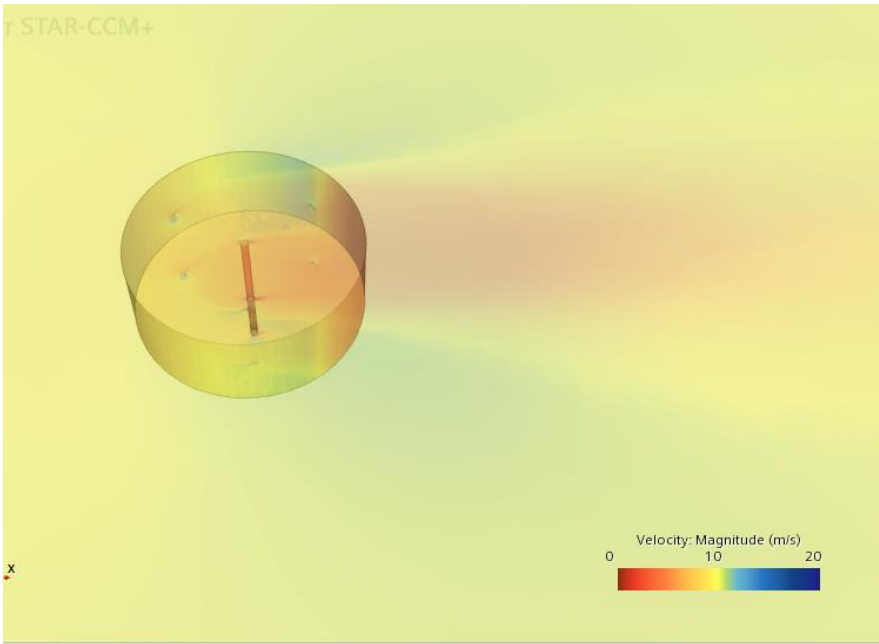
Figure 19: Figure shows the Velocity profile of the 3D configuration under consideration; the figure is obtained from the transparent view under Star CCM+. the rotating and stationary domain be clearly seen.
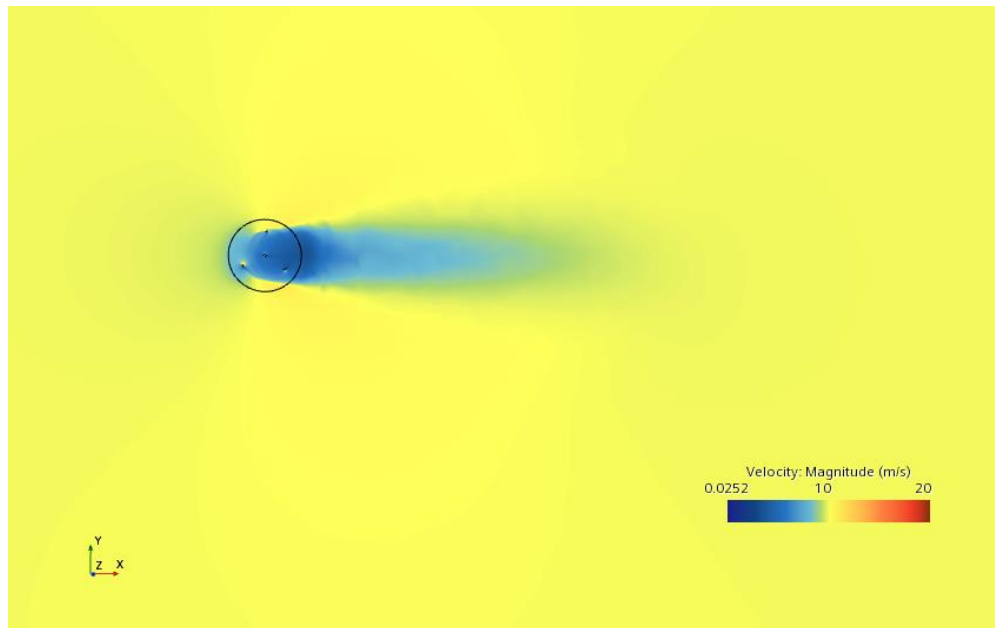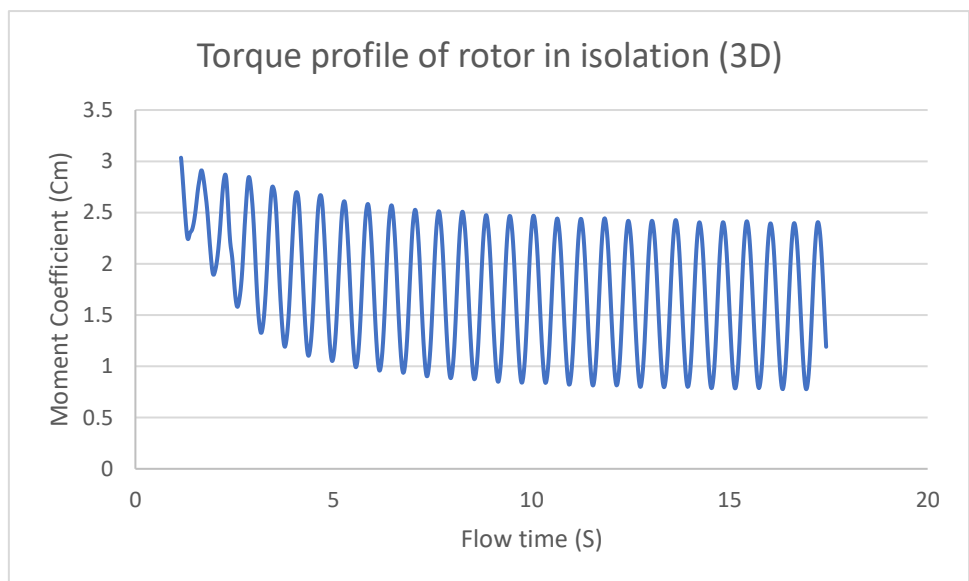

Figure 20: Figure shows the Velocity profile of (sectional view) of the 3D configuration. The cross-sectional view of the velocity profile is similar to 2D velocity profile.

Figure 21: Torque profile experienced by the rotor (3D) over the flow time, as we can see the moment coefficient has increased promotionally comparing with figure 16.

From (Eq.8) Moment coefficient: Cm = M / (0.5 ρ AV2)

Where: Moment coefficient = Cm M = The body's or structure's moment or torque ρ = the air density A = Area of reference V = Wind speed

The body's or structure's moment or torque can be calculated by multiplying the moment arm (l) by the lift coefficient (Cl). The lift coefficient and the moment arm are commonly used to form the following expression for the moment:

M = Cl * l

    (Eq.11)

From the above equations it is possible to assume that the moment coefficient can be calculated by simply multiplying it by the blade length (height of the blade) if the 2D analysis yields precise lift coefficients and the moment arm is mostly driven by the vertical height of the blade. It is crucial to keep in mind that this strategy also assumes that the moment coefficient is not considerably impacted by the spanwise flow changes and other three-dimensional flow effects. The 3D analysis is conducted to compare the results of the 2D simulation. It was found that the moment coefficient increases as the length of the blade has increased. The average moment coefficient under 3D analysis is found to be 1.632. The average moment coefficient under 2D analysis was 0.137. It can be derived from the above results that the increase in moment coefficient under 3D analysis is 12 times as that of a 2D analysis.in a 2D analysis the height is assumed to be unity. The

3D Vertical axis wind turbine had a blade height of 12m. It can be understood that the moment coefficient has just increased in a proportional manner to the blade length. The velocity profiles were also studied and the cross-sectional view of the velocity profile of the 3D vertical axis wind turbine is like that of the velocity profile of the 2D analysis.

It was also noted from the 3D analysis that the computational time also increases corresponding to the increase in the blade length. Therefore, it is more practical to conduct a 2D analysis and the moment coefficient can be directly multiplied by the blade length to get the moment coefficient under 3D analysis. It was also verified that the 2D results and the 3D results are well in tantum with each other.

4.2 Two rotor systems
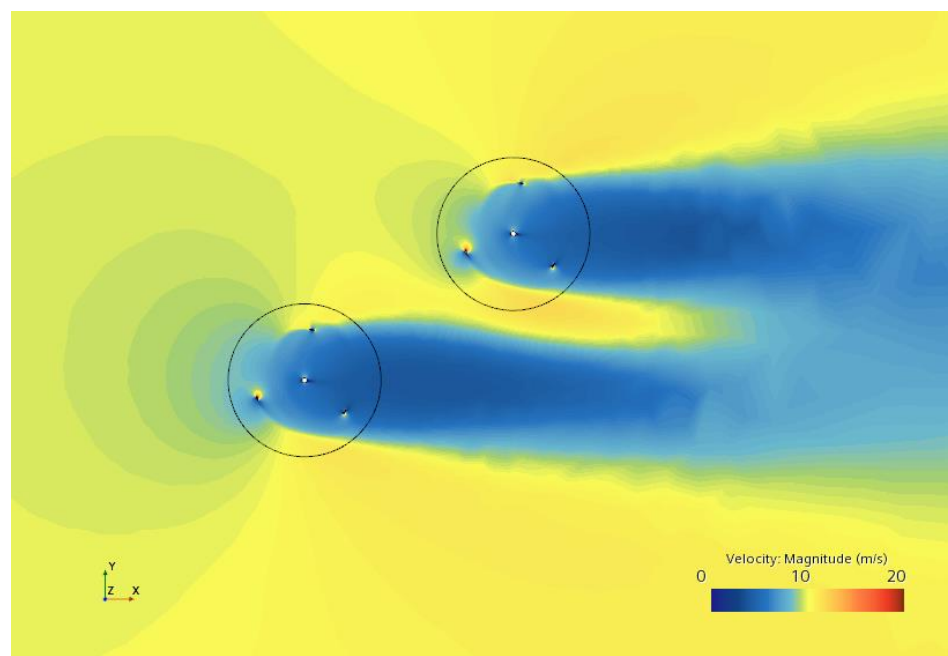
Figure 22: Figure shows the Velocity profile of the configuration under consideration.

Figure 23: Distribution of the rotors are arranged in the array and how they are numbered, it is important to number the rotor in order to identify the performance of each to the performance of the system. Here in this case, there are two rotors in the system placed at an angle of $60°$.
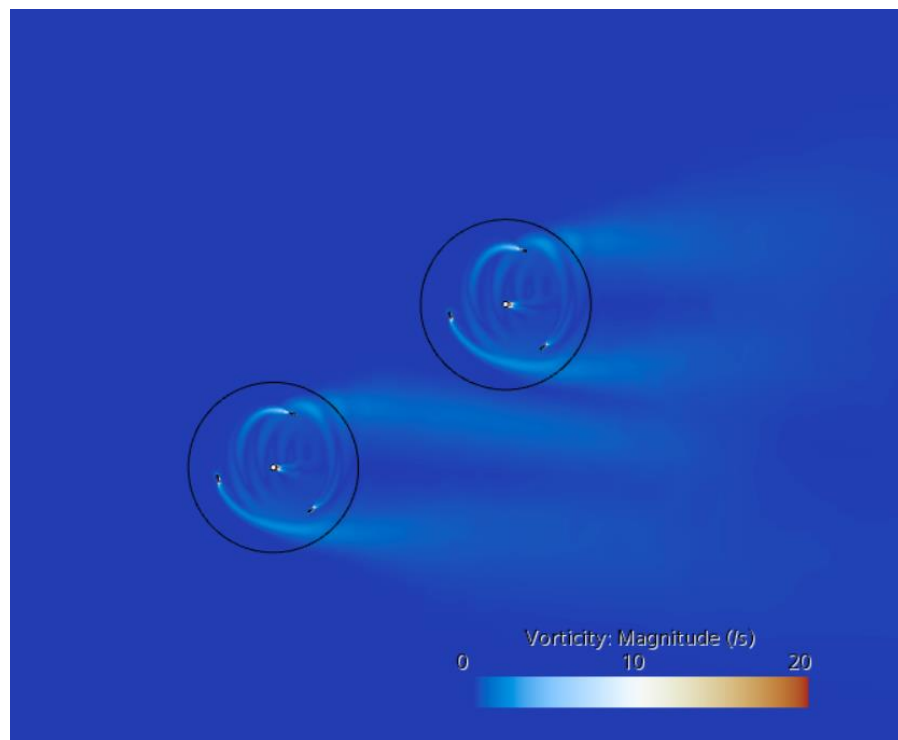
Figure 24: Figure shows the Vorticity profile of the configuration under consideration.
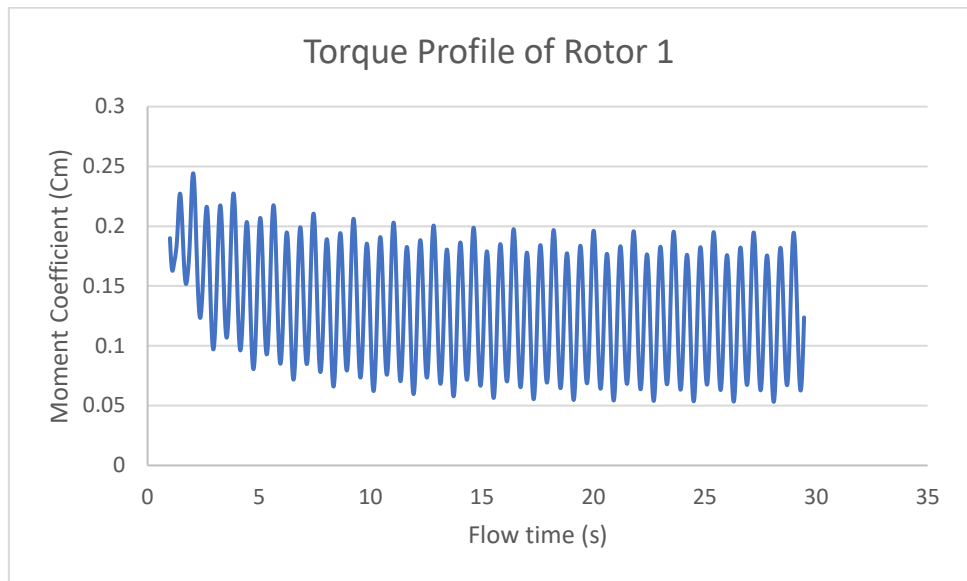
Figure 25: Torque profile experienced by the rotor 1 over the flow time. The position of rotor 1can be identified from the figure 23
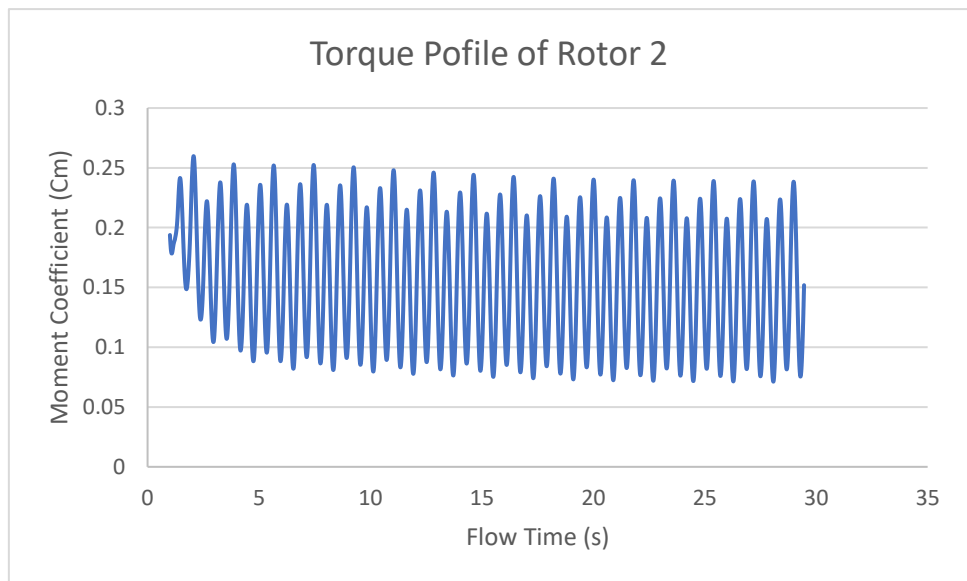
Figure 26: Torque profile experienced by the rotor 2 over the flow time. The position of rotor 2 can be identified from the figure 23

The creation of vortices, which may enhance or adversely impact performance, is revealed by vorticity plots. The rotors' ability to capture energy can be enhanced by clearly defined vortices. However,

excessive or irregularly positioned vortices can cause turbulence, boost drag, and hinder performance. Unsteady flow patterns are produced when vortices separate from the rotor surface and shed into the wake. For minimizing rotor interactions and maximizing energy extraction, vortex shedding must be managed properly. The vortices formed, (Figure 24) for this configuration has enhanced the efficiency of the VAWT farm. Figure 22: Figure shows the Velocity profile of the configuration under consideration.

Figure 23 shows the distribution of the rotors arranged in the array and how they are numbered. It is important to number the rotor in order to identify the performance of each to the performance of the system. Here in this case, there are two rotors in the system placed at an angle of $60°$.Figure 25 shows torque profile experienced by rotor 1 over the flow time. Figure 26 shows torque profile experienced by rotor 2 over the flow time.

From the studies conducted by [15] Hansen et.al, it was identified that rotors when placed at angle of $60°$ will produce maximum efficiency. This study tries to incorporate a greater number of rotors and maneuver the rotors over various configurations to produce maximum result. The next step was to construct a two-rotor system. The second rotor was placed at 2D, D represents the diameter, and at an angle of $60°$. The performance indicator value for the combined two rotor system was about 1.054. The performance coefficient did not increase much which made it necessary to introduce one more rotor and construct a three-rotor system. The average moment Coefficient value is 0.138 and the average power coefficient is 0.472 for rotor 1. The average moment Coefficient value is 0.159 and the average power coefficient is 0.54 for rotor 2. The performance of the second rotor has increased to a certain limit without compromising on the performance of the first. This has led to the overall increase in the performance indicator of 5.4%.

4.3 Three rotor systems

When several rotors are arranged in a triangle, the wakes produced by one rotor may interact with the others, reducing the incoming wind velocity for downstream rotors. Because there is less kinetic energy in the wake zone, efficiency may suffer as a result. However, the wake interference may be reduced, enabling each rotor to function in undisturbed wind, boosting total efficiency. This can be accomplished by correctly aligning and spacing the rotors. Vorticity, which describes the rotational motion of fluid particles, may be created in the flow by the interaction of many rotors in a triangle arrangement. The vorticity created; Figure 29 here has enhanced the performance of the turbine. It assists in spreading the wind's momentum, boosting the pressure differential between the two sides of the rotor, and thereby enhancing the power output of Rotor 2.
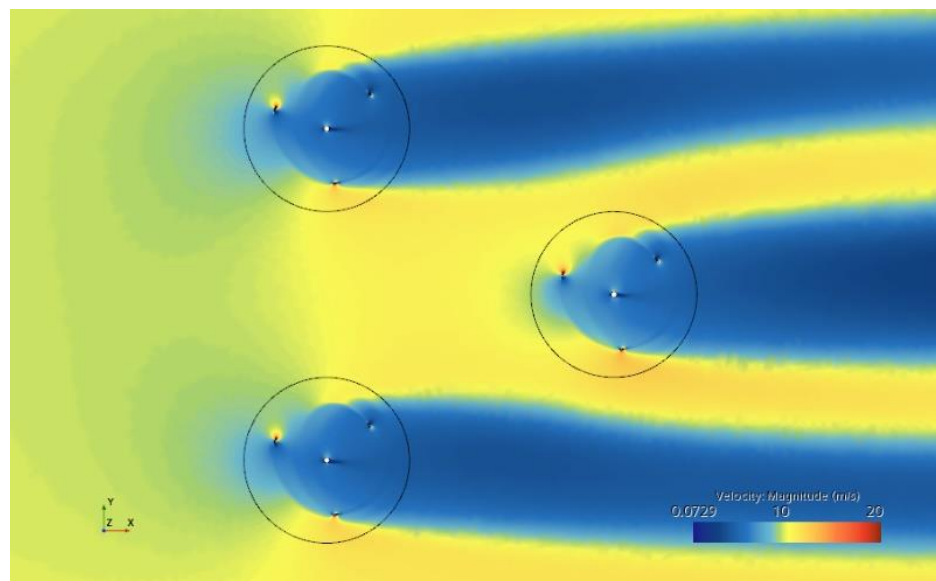
Figure 27: Figure shows the Velocity profile of the configuration under consideration, 3 rotor triangle configurations.

Figure 28: Distribution of the rotors are arranged in the array and how they are numbered, it is important to number the rotor in order to identify the performance of each to the performance of the system. Here in this case there are three rotors, like a triangle converging to the freestream at the inlet placed at an angle of $60°$.

Figure 29: Figure shows the Vorticity profile of the configuration under consideration , 3 rotor triangle configuration.
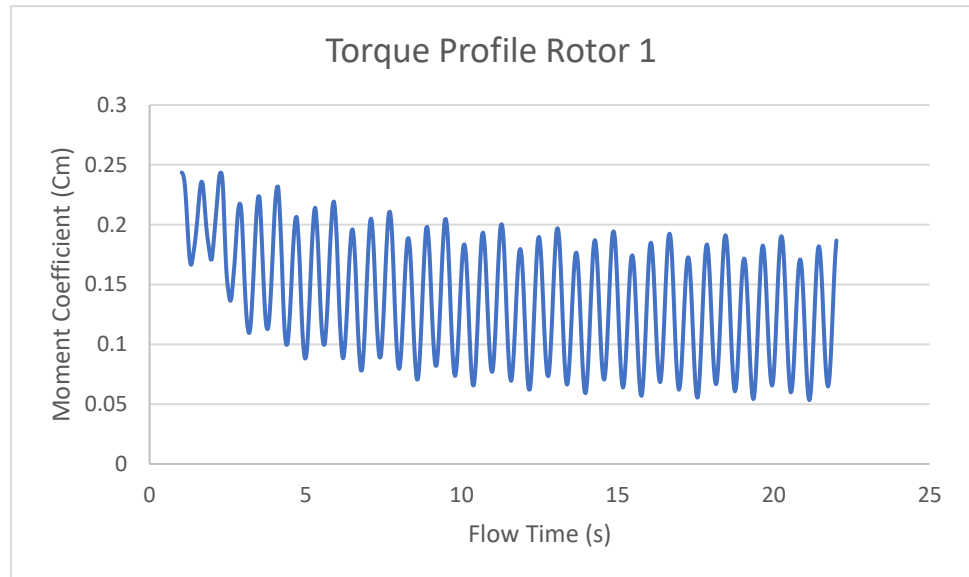
Figure 30: Torque profile experienced by the rotor 1 over the flow time. The position of rotor 1 can be identified from figure 28.
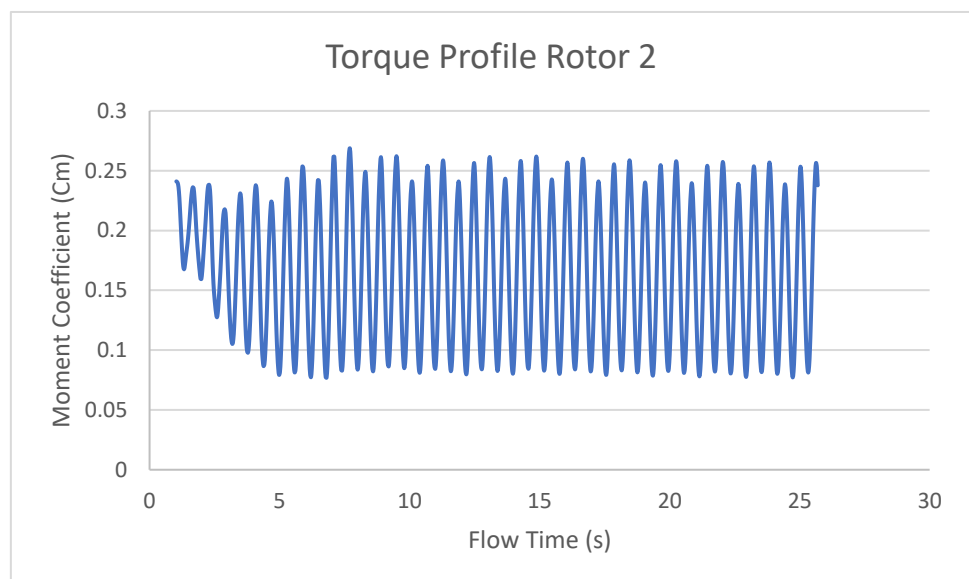
Figure 31: Torque profile experienced by the rotor 2over the flow time. The position of rotor 2 can be identified from figure 28. The moment coefficient of Rotor 2 shows and increases compared to the other two rotors.
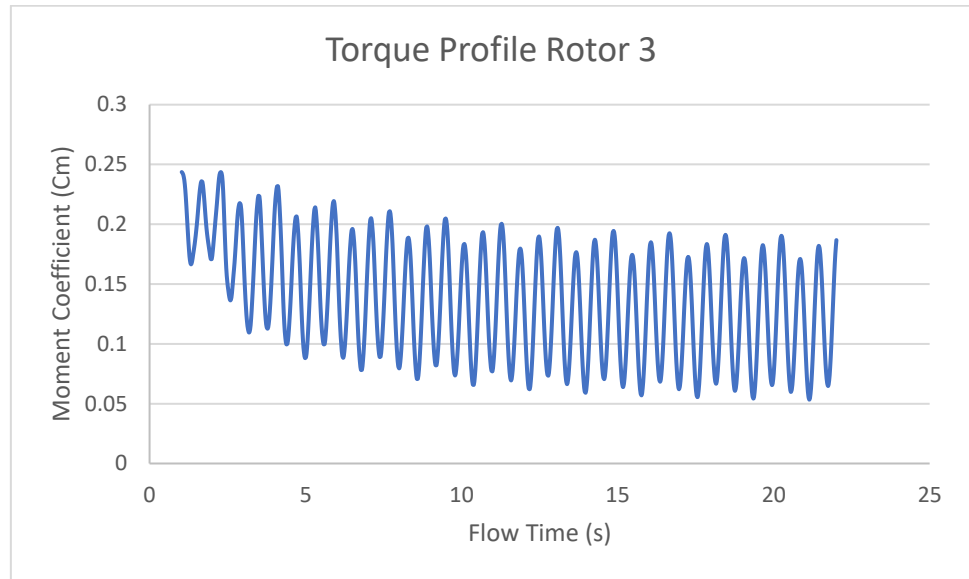
Figure 32 Torque profile experienced by the rotor 3 over the flow time. The position of rotor 3 can be identified from figure 28.

Figure 28 shows the distribution of the rotors arranged in the array and how they are numbered. It is important to number the rotor in order to identify the performance of each to the performance of the system. Here in this case, there are three rotors, like a triangle converging to the freestream at the inlet placed at an angle of 60°.Figure 30orque profile experienced by the rotor 1 over the flow time.

Figure 31 shows torque profile experienced by rotor 2 over the flow time. The moment coefficient of Rotor 2 shows and increases compared to the other two rotors. Figure 32 shows torque profile experienced by rotor 3 over the flow time. From the Figure 27 it can be identified that formation of rotors and the effect of the wake field has led to a venturi effect, which is one of the reasons by which the air passes through a converging section just like a nozzle, which results in the reduction of area and increase in the velocity, this has improved the performance coefficient to value of 1.14. The average moment

Coefficient value was 0.153 and the average power coefficient was 0.535 for rotor 1 The average moment Coefficient value was 0.163 and the average power coefficient is 0.570 for rotor 2 The average moment Coefficient value is 0.153 and the average power coefficient is 0.535 for rotor 3. The performance of the second rotor has increased to a certain limit without compromising much on the performance of the other two. This led to the overall increase in performance indicator of 14%. Roto1 and rotor 3 have a similar value for power coefficient and moment coefficient, this might be due to the symmetry in geometry, but the performance characteristics of the rotor at the end (rotor 2) has slightly increased.
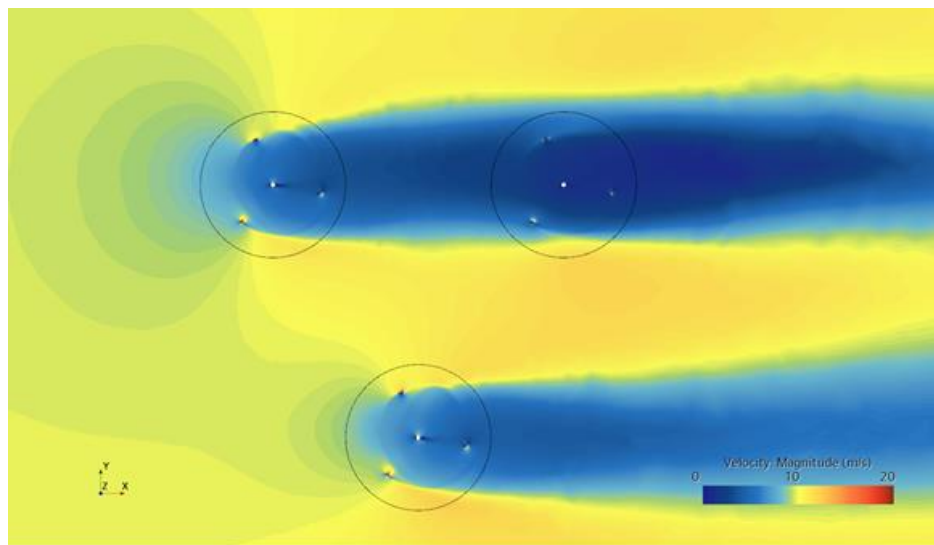
Figure 33: Figure shows the Velocity profile of the configuration under consideration.

Figure 34: Distribution of the rotors are arranged in the array and how they are numbered, it is important to number the rotor in order to identify the performance of each to the performance of the system. Here in this case there are three rotors, like a triangle rotor one is in line with rotor two, rotor 3 is placed at an angle of 60°
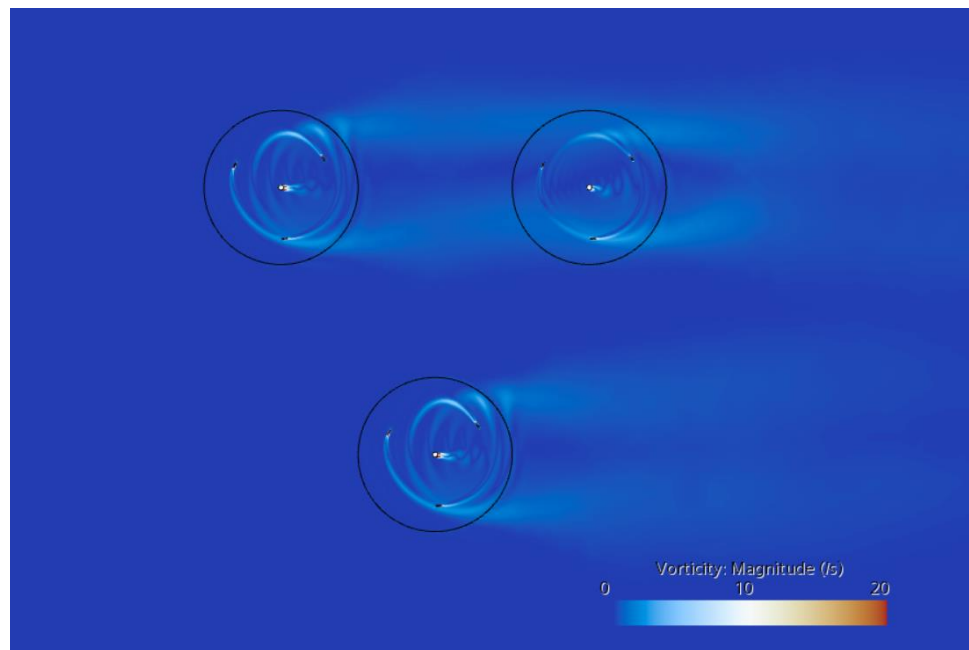
Figure 35: Figure shows the Vorticity profile of the configuration under consideration.

A fluid element's local spinning motion or circulation is measured by a property called vorticity Figure 35. Vorticity plots show the

development of vortices and eddies around the rotors and in the wake area in the context of a VAWT system. A certain degree of vorticity is added to the flow as the wind hits the first rotor. Rotor 1 causing the blockage effect to Rotor 2 has reduced the vortices formed in Rotor 2 and in turn led to decreased efficiency.
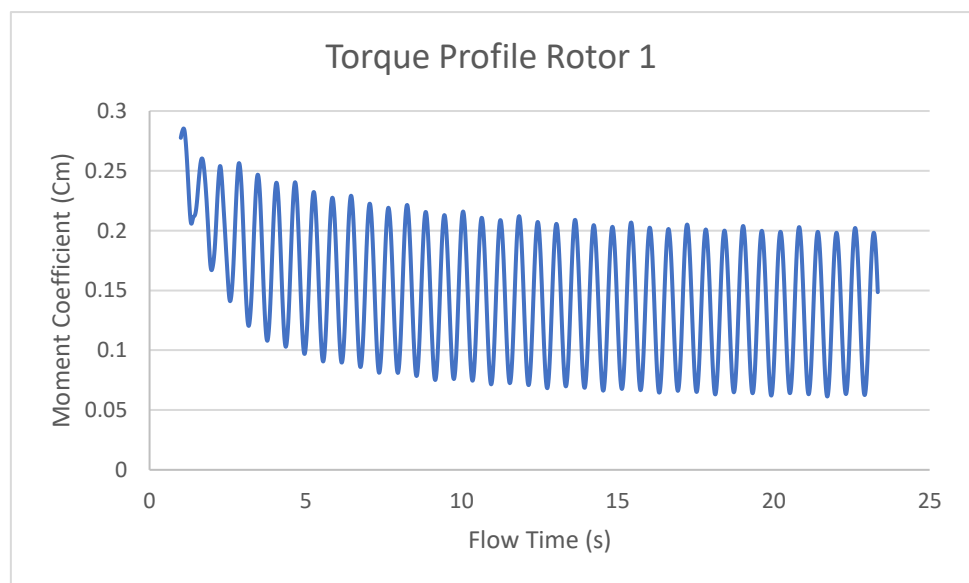
Figure 36: Torque profile experienced by the rotor 1 over the flow time.
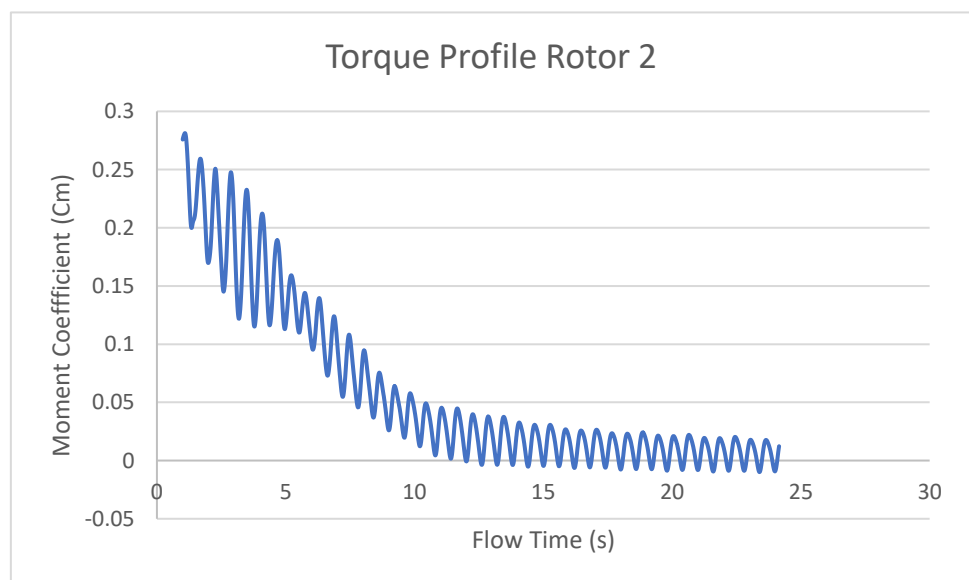
Figure 37: Torque profile experienced by rotor 2 over the flow time. Moment Coefficient decreases steadily after the wake filed (low velocity) reaches the vicinity of rotor 2.
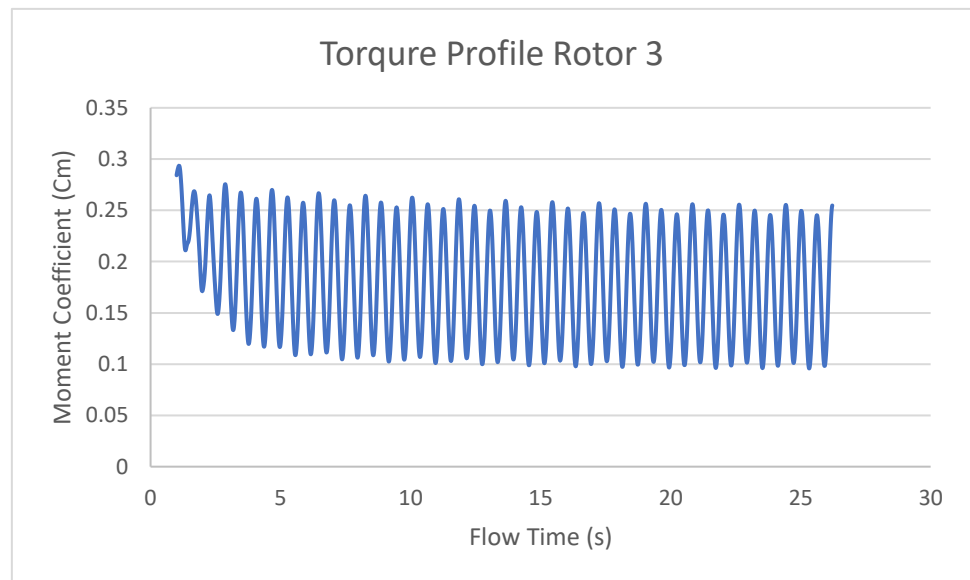
Figure 38: Torque profile experienced by rotor 3 over the flow time.

Figure 34 shows the distribution of the rotors arranged in the array and how they are numbered, it is important to number the rotor in order to identify the performance of each to the performance of the system. Here in this case, there are three rotors, like a triangle rotor one is in line with rotor two, rotor 3 is placed at an angle of 60°

Figure 36 shows torque profile experienced by rotor 1 over the flow time. Figure 37 shows the torque profile experienced by rotor 2 over the flow time. Moment Coefficient decreases steadily after the wake filed (low velocity) reaches the vicinity of rotor 2. Figure 38 shows the torque profile experienced by rotor 3 over the flow time. On the other hand, figure 33 shows the velocity profile of a three-turbine system in which one of the rotors is placed at distance of 2D distance behind the

first one and it is in line making no angle, this rotor obstructs the air and to pass directly through its blades. The low velocity wakes from the first rotor affects the efficiency of the second rotor and reduces the torque to a great extent after the flow reaches the vicinity. This caused the performance coefficient to reduce to 0.96 in the second case. The average moment Coefficient value was 0.145 and the average power coefficient was 0.507 for rotor 1. The average moment Coefficient value was 0.058 and the average power coefficient is 0.203 for rotor 2 The average moment Coefficient value is 0.184 and the average power coefficient is 0.644 for rotor 3. The performance of the second rotor has decreased as explained earlier, even though rotor 3 had good performance characteristics, this has led to the overall decrease in performance indicator of 4%. Figure 31 shows clearly how the Moment Coefficient decreases steadily after the wake field (low velocity) reaches the vicinity of rotor 2.
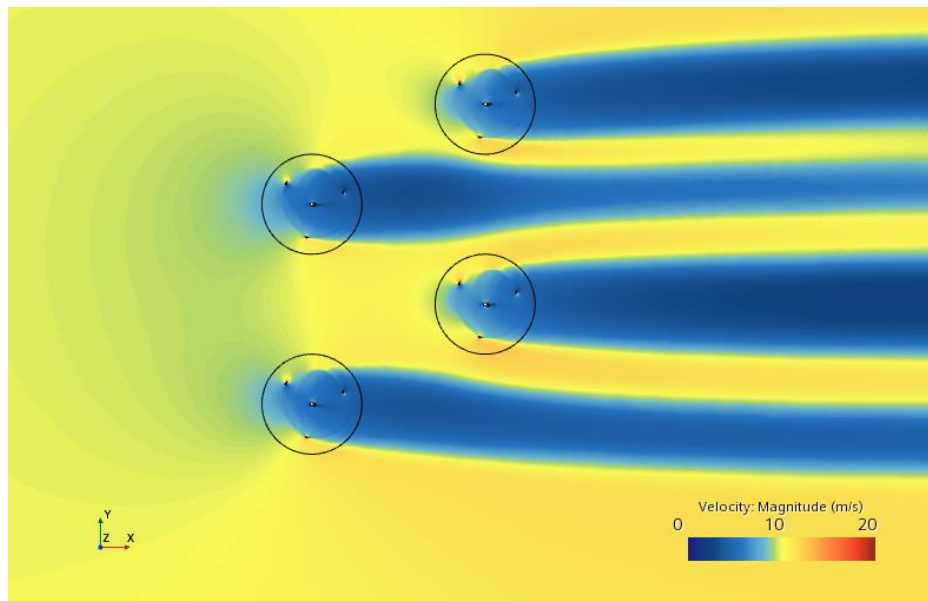
4.4 Four rotor systems

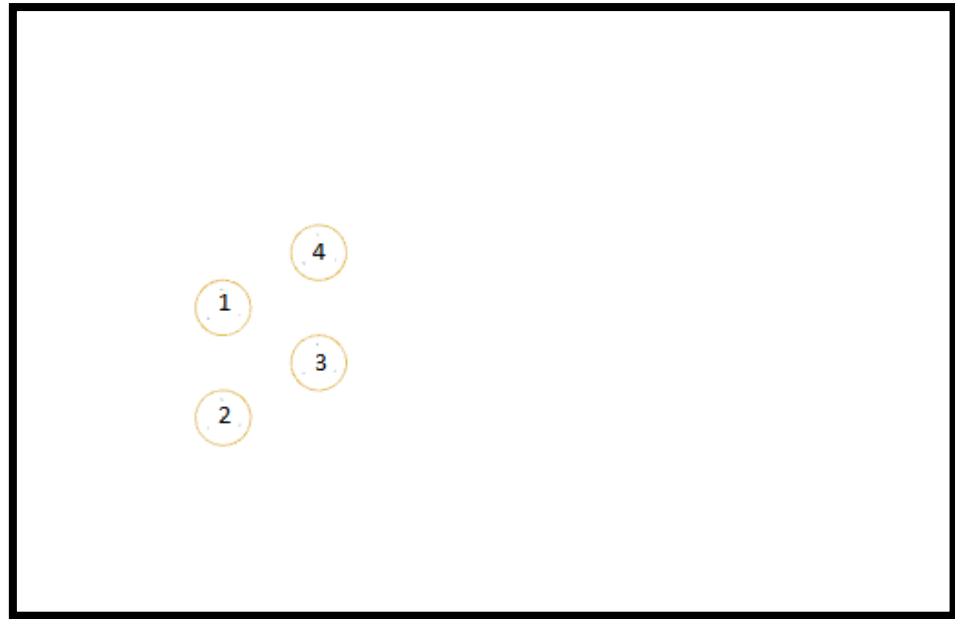Figure 39: Figure shows the Velocity profile of the configuration under consideration.

Figure 40: Distribution of the rotors are arranged in the array and how they are numbered, it is important to number the rotor in order to identify the performance of each to the performance of the system. Here in this case, there are four rotors, like a rhombus placed at an angle of $60°$.
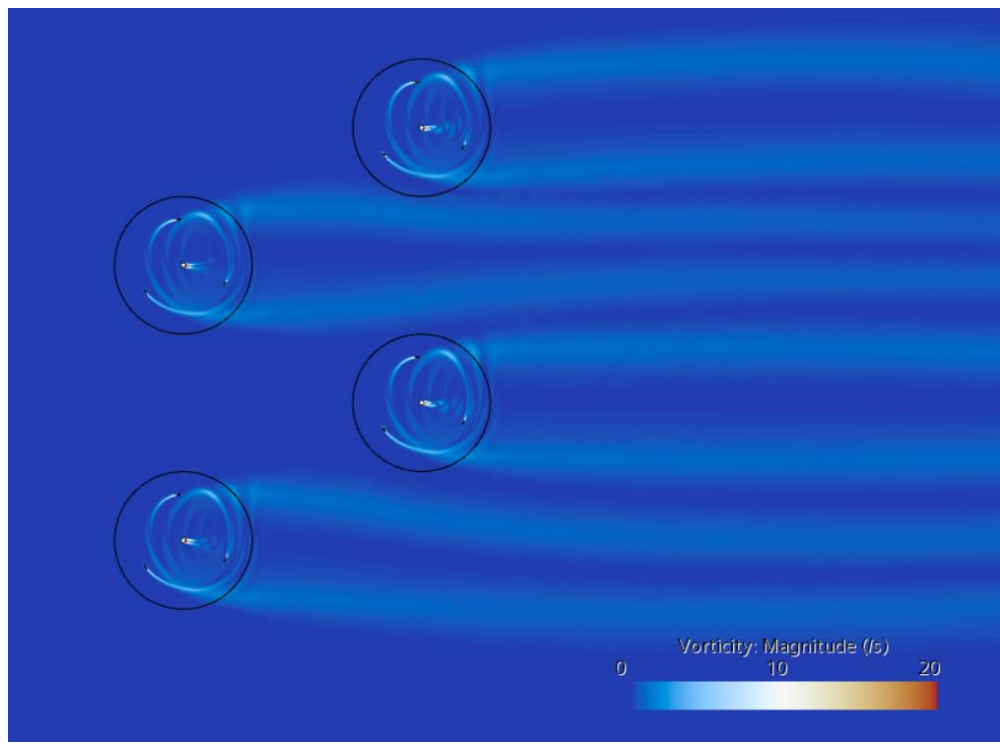

Figure 41: Figure shows the Vorticity profile of the configuration under consideration.
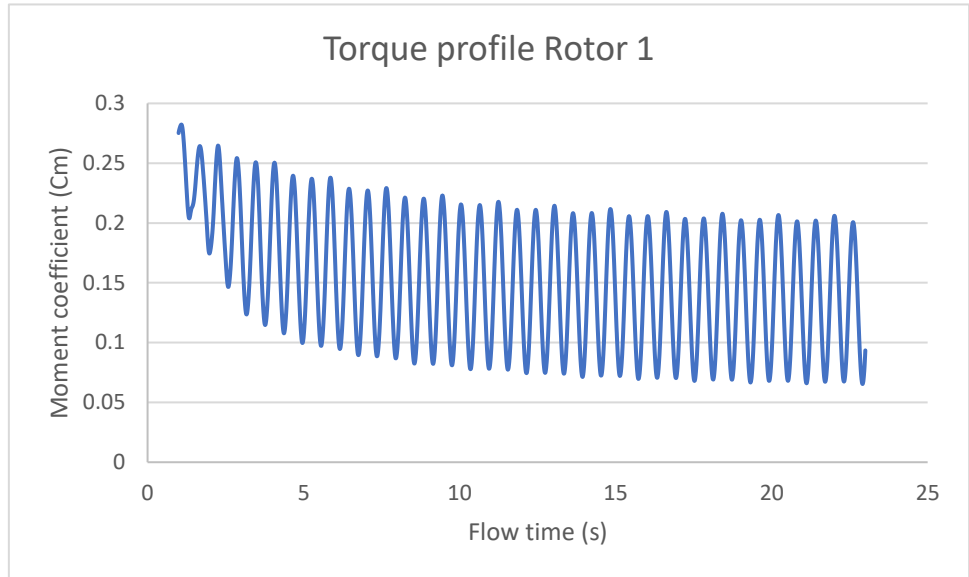
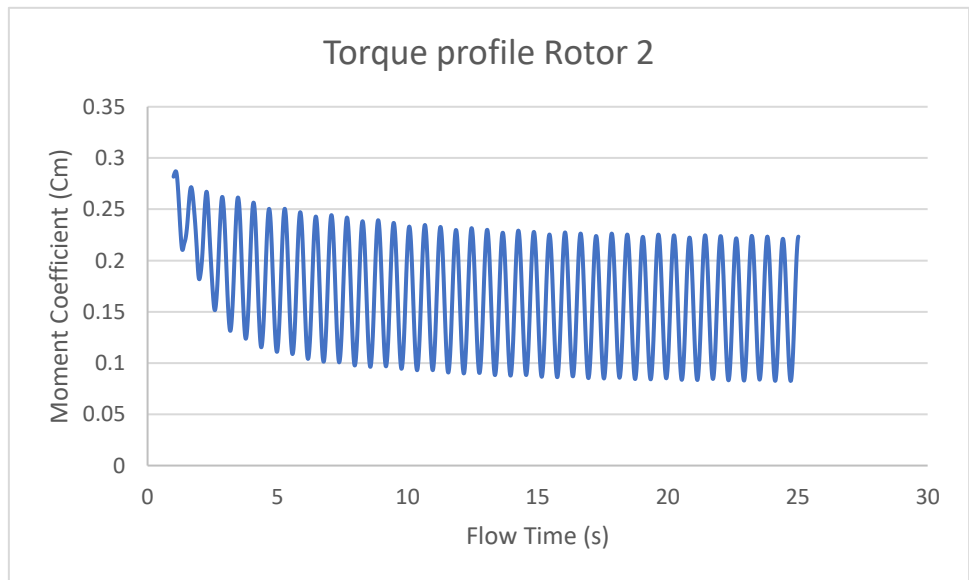Figure 42: Torque profile experienced by rotor 1 over the flow time.

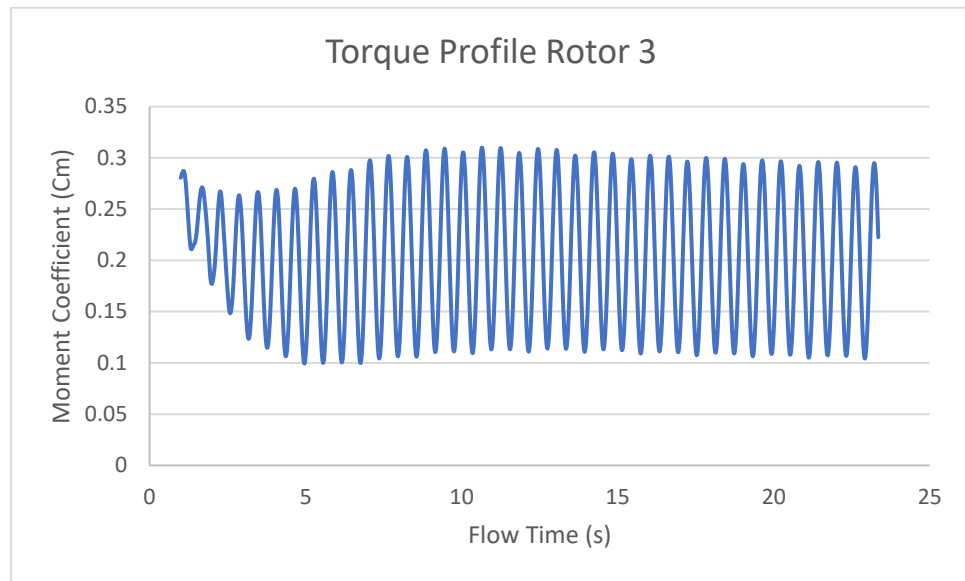Figure 43: Torque profile experienced by rotor 2 over the flow time.

Figure 44: Torque profile experienced by the rotor 3 over the flow time. The moment coefficient of Rotor 2 shows and increase compared to the other rotors.
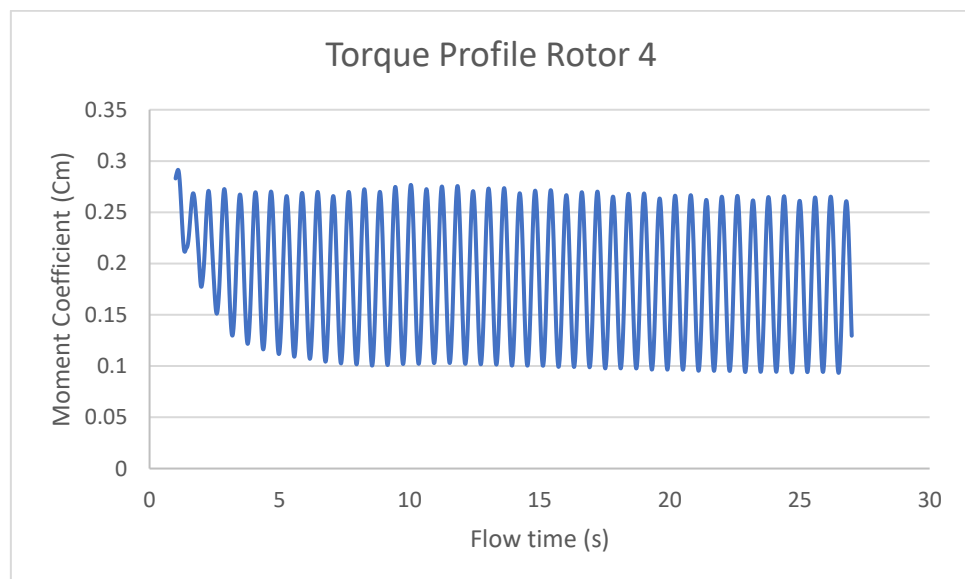

Figure 45: Torque profile experienced by rotor 4 over the flow time.

The next step was to try the simulation with a four-rotor system (rhombus configuration). Figure 33 shows the velocity profile of four rotors placed at 60° and no rotors are blocking each other in the wind direction. Figure 40: Distribution of the rotors are arranged in the array and how they are numbered, it is important to number the rotor in order

to identify the performance of each to the performance of the system. Here in this case, there are four rotors, like a rhombus placed at an angle of 60°.Figure 41 shows the Vorticity profile of the configuration under consideration. Figure 42,43,44,45 shows the torque profile experienced by the rotor 1,2,3,4 respectively over the flow time.

The results obtained so far have encouraged to try one more rotor like rhombus situation. The converging triangle configuration obtained a 14 % increase, placing one more rotor will provide a rhombus as shown in figure 33. The performance indicator value also increased to 1.34, when compared to triangle configuration. The average moment Coefficient value was 0.154 and the average power coefficient was 0.539 for rotor 1. The average moment Coefficient value was 0.173 and the average power coefficient is 0.60 for rotor 2. The average moment Coefficient value is 0.2057 and the average power coefficient is 0.717 for rotor 3. The average moment Coefficient value is 0.190 and the average power coefficient is 0.665 for rotor 4. The performance of the third rotor has increased as explained earlier, rotor 3 had good performance characteristics, this has led to the overall increase in performance indicator of 34%. Figure 36 shows clearly how the Moment Coefficient increases, and the average value reached above 0.2 for the first time. It can lower a turbine's efficiency if the wake field behind it is fully or partially blocked by other turbines or any other object. The area of disrupted airflow that develops downstream of a turbine as a result of the interaction between the revolving blades and the wind is referred to as the wake field. Rotor 1 may experience higher air turbulence and turbulence due to the presence of Rotor 3 and Rotor 4 in the wake field. Turbulence increases the drag on the blades, making it harder for the turbine to keep turning. The turbine's overall efficiency may suffer as a result of the higher drag. The greater drag requires more energy to overcome, which lowers the turbine's net power output. On the other hand, Rotor 2 has only rotor 3 obstructing

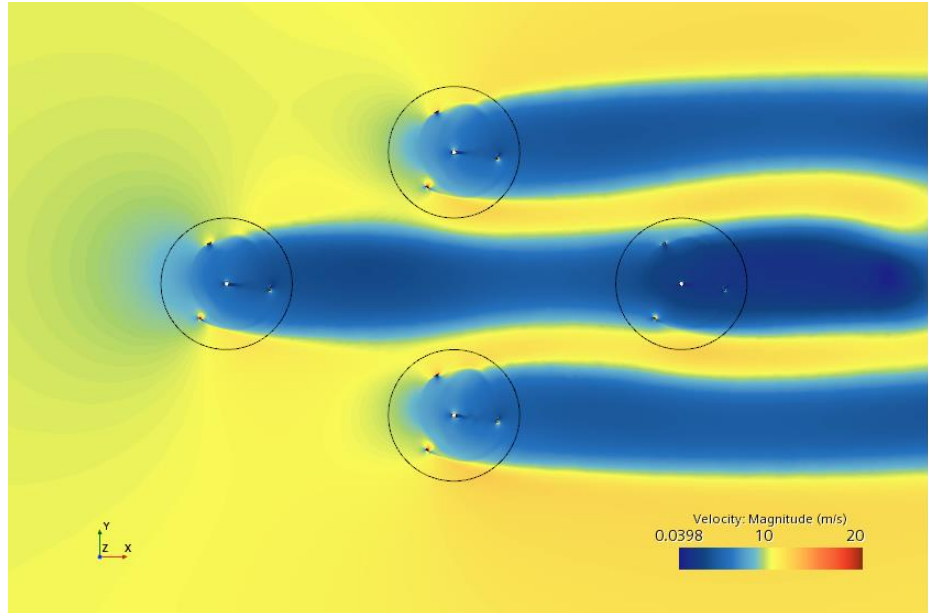the wake field behind it. That is why Rotor 2 has slightly higher efficiency than Rotor 1. [51]

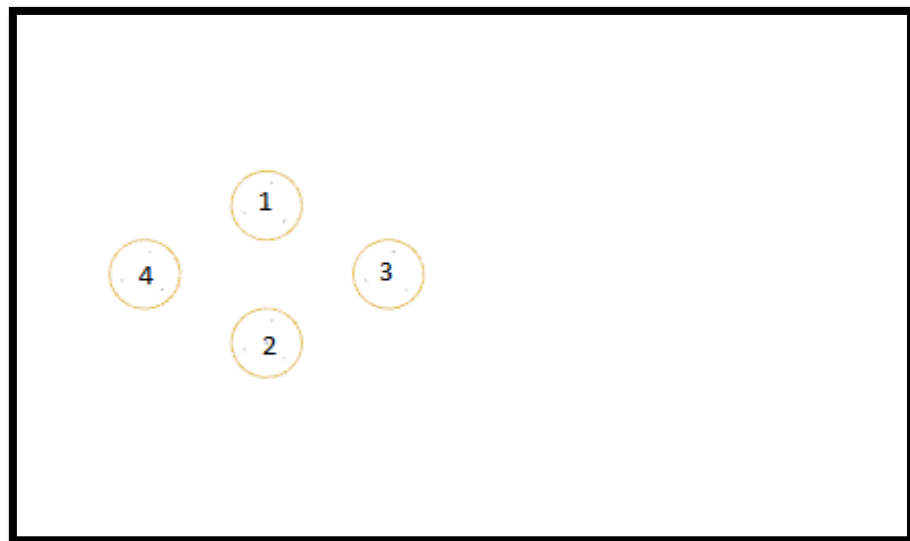Figure 46: Figure shows the Velocity profile of the configuration under consideration.

Figure 47: Distribution of the rotors are arranged in the array and how they are numbered, it is important to number the rotor in order to identify the performance of each to the performance of the system. Here in this case there are four rotors, like a rhombus rotor four is in line with rotor three.
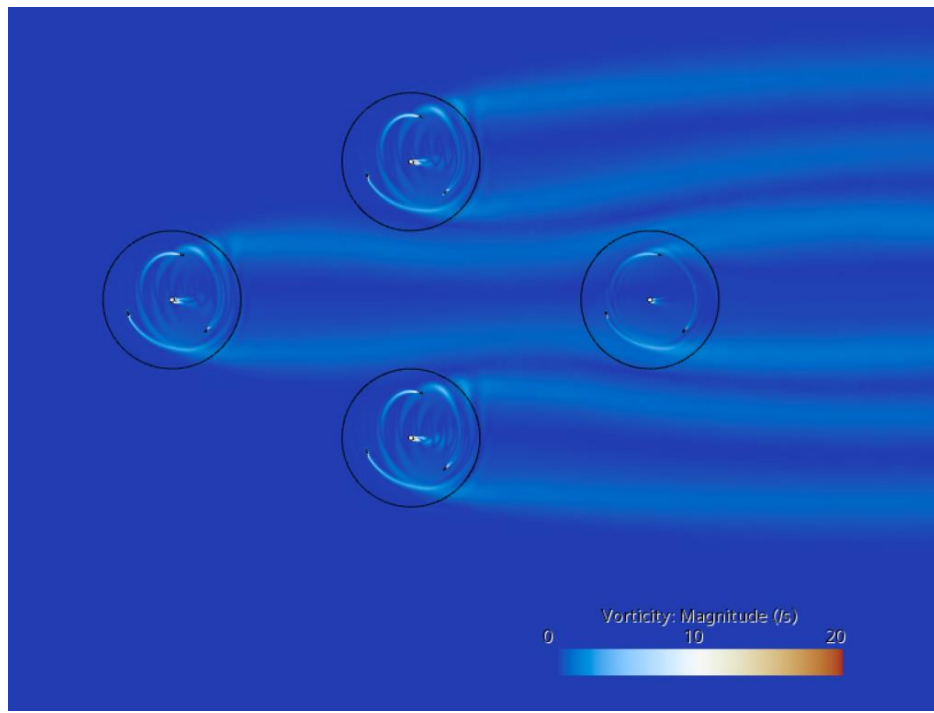
Figure 48: Figure shows the Vorticity profile of the configuration under consideration.
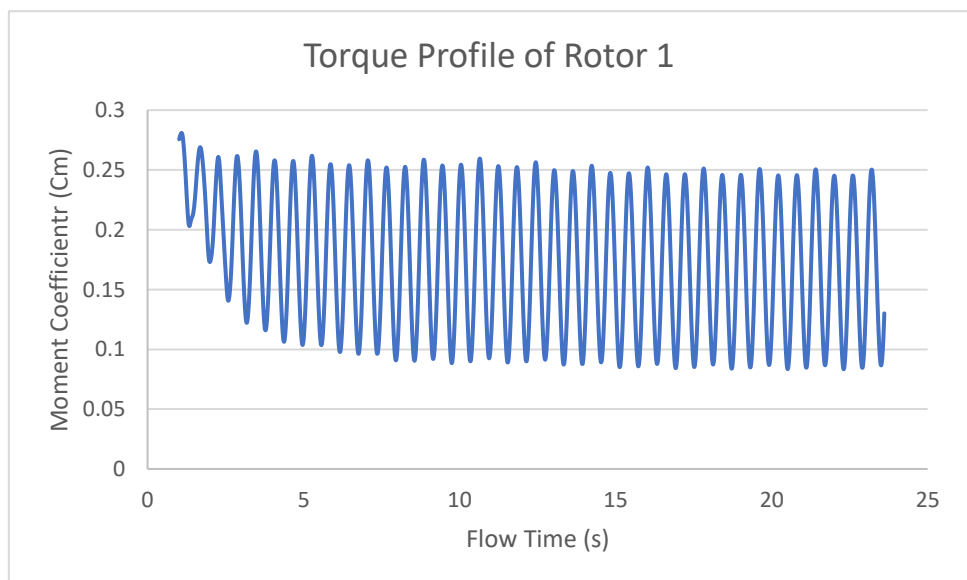

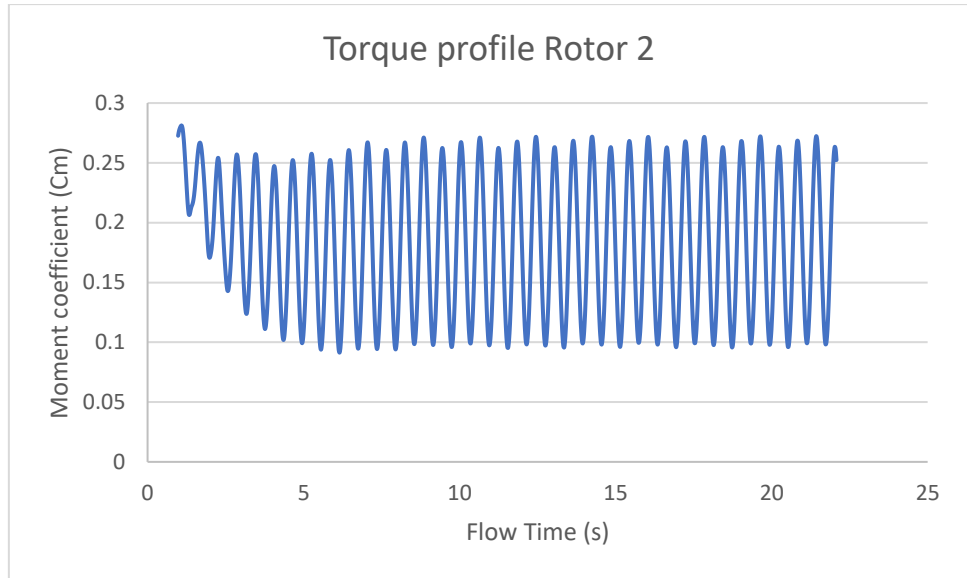Figure 49: Torque profile experienced by the rotor 1 over the flow time.

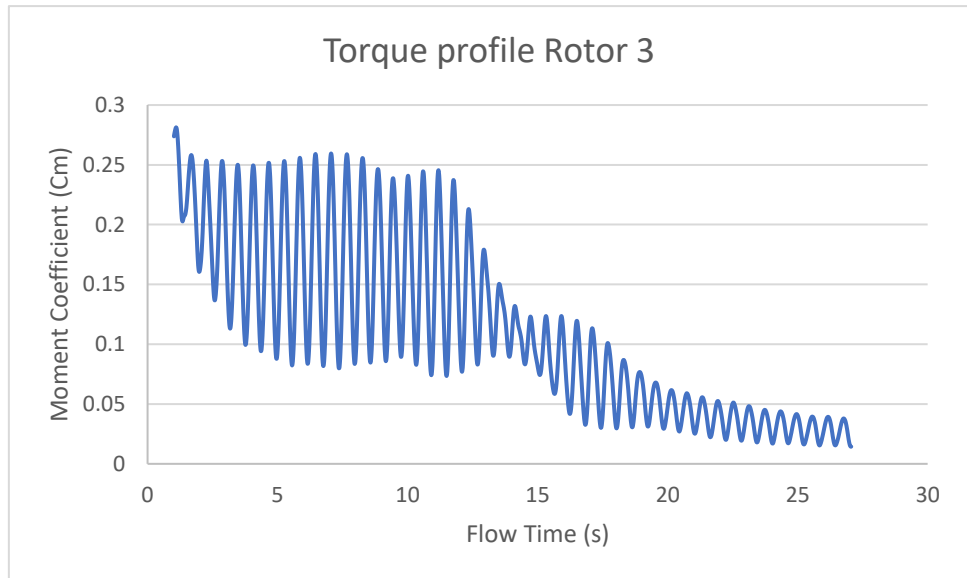Figure 50: Torque profile experienced by rotor 2 over the flow time.

Figure 51: Torque profile experienced by the rotor 3 over the flow time. Moment Coefficient decreases steadily after the wake filed (low velocity) reaches the vicinity of rotor 3.
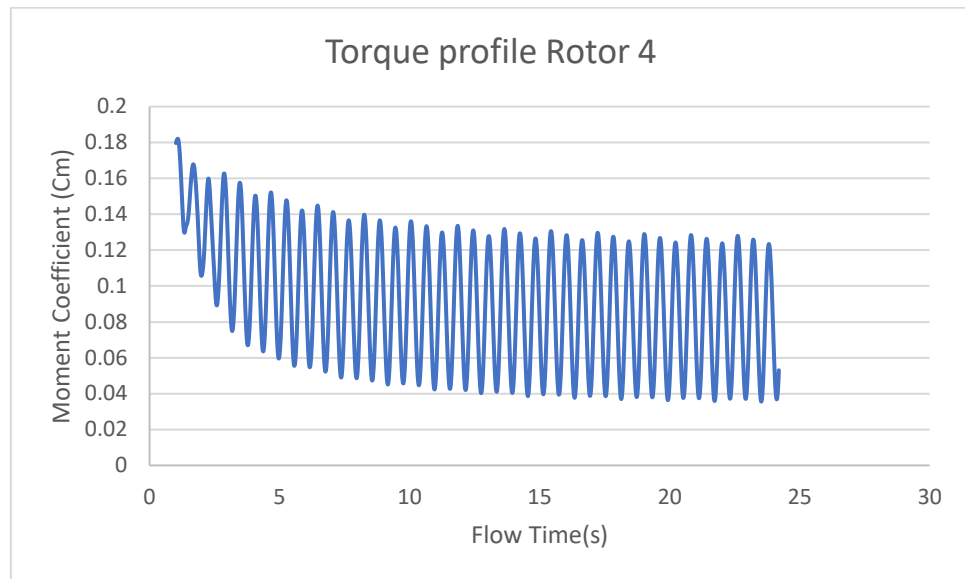
Figure 52: Torque profile experienced by the rotor 4 over the flow time.

Figure 46 shows the Velocity profile of the configuration under consideration. Figure 47 shows the distribution of the rotors arranged in the array and how they are numbered. It is important to number the rotor in order to identify the performance of each to the performance of the system. Here in this case, there are four rotors, like a rhombus rotor four is in line with rotor three. Figure 48 shows the Vorticity profile of the configuration under consideration. Figure 49,50,51,52 shows Torque profile experienced by the rotor 1, rotor 2, rotor 3, rotor 4 respectively over the flow time.

The performance increase of a rhombus configuration has encouraged to try a different orientation using the same configuration. The second configuration with a Rotor 3 system placed in such a manner that it is in line with the Rotor 4 as expected produced a lesser performance indictor value of 0.93, due to the blockage effect. Rotor 3 gets affected

by the low velocity wake field created by the Rotor 4. From this it can be concluded that it is not efficient to place rotors colinear to each other in the direction of air flow. The low velocity wakes from R4 affects the efficiency of the R3 and reduces the torque to a great extent after the flow reaches the vicinity. This caused the performance coefficient to reduce to 0.93. As explained earlier It can lower a turbine's efficiency if the wake field behind it is fully or partially blocked by other turbines or any other object. Additional drag and airflow disturbance may result if the first turbine's wake field immediately impacts the second turbine's blades. The performance and efficiency of both turbines may suffer as a result of this interaction. Here Rotor 4 fully blocks Rotor 1 and it impacts the efficiency. [51] The average moment Coefficient value was 0.171 and the average power coefficient was 0.598 for rotor 1. The average moment Coefficient value was 0.183 and the average power coefficient is 0.64 for rotor 2. The average moment Coefficient value is 0.0712 and the average power coefficient is 0.249 for rotor 3. The average moment Coefficient value is 0.0862 and the average power coefficient is 0.301 for rotor 4. The performance of the second R3 has decreased as explained earlier, even though rotor 2 had good performance characteristics, this has led to the overall decrease in performance indicator of 7%. Figure 51 shows clearly how the Moment Coefficient decreases steadily after the wake filed (low velocity) reaches the vicinity of rotor 3.
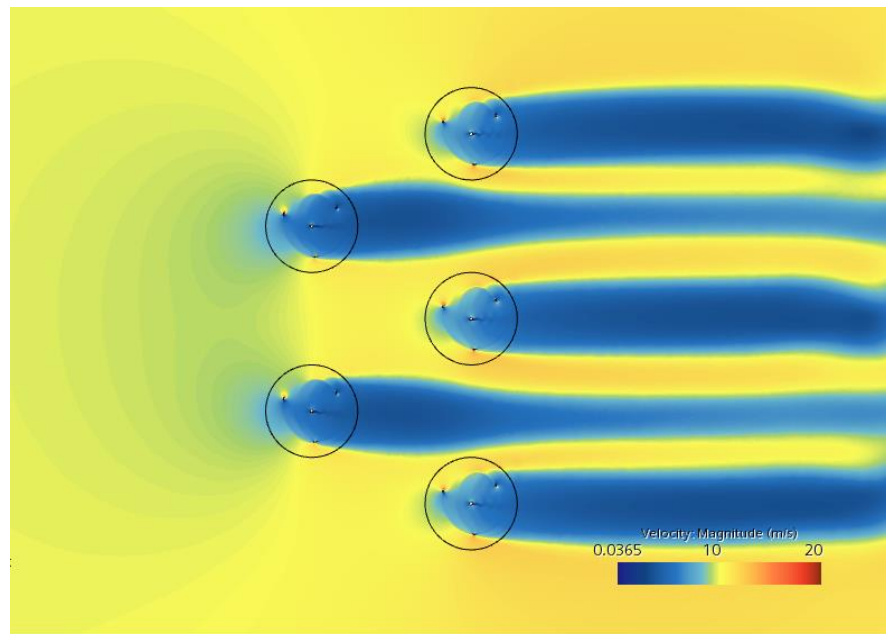
4.5 Five rotor systems

Figure 53: Figure shows the Velocity profile of the configuration under consideration.

Figure 54: Distribution of the rotors are arranged in the array and how they are numbered, it is important to number the rotor in order to identify the performance of each to the performance of the system. Here in this case there are five rotors, like a staggered configuration placed at an angle of $60°$
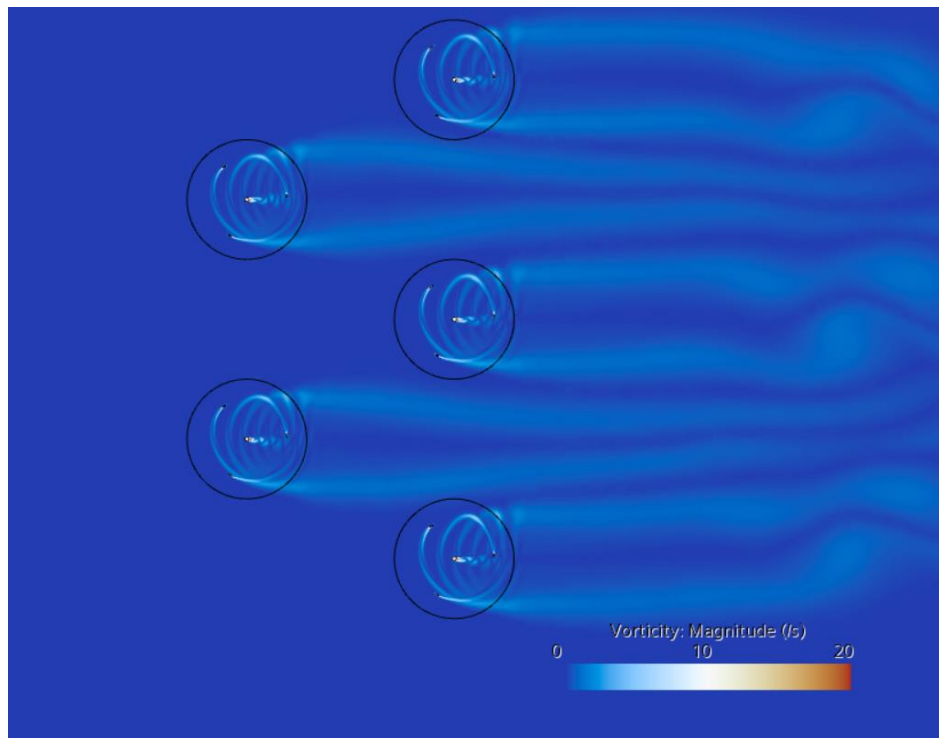

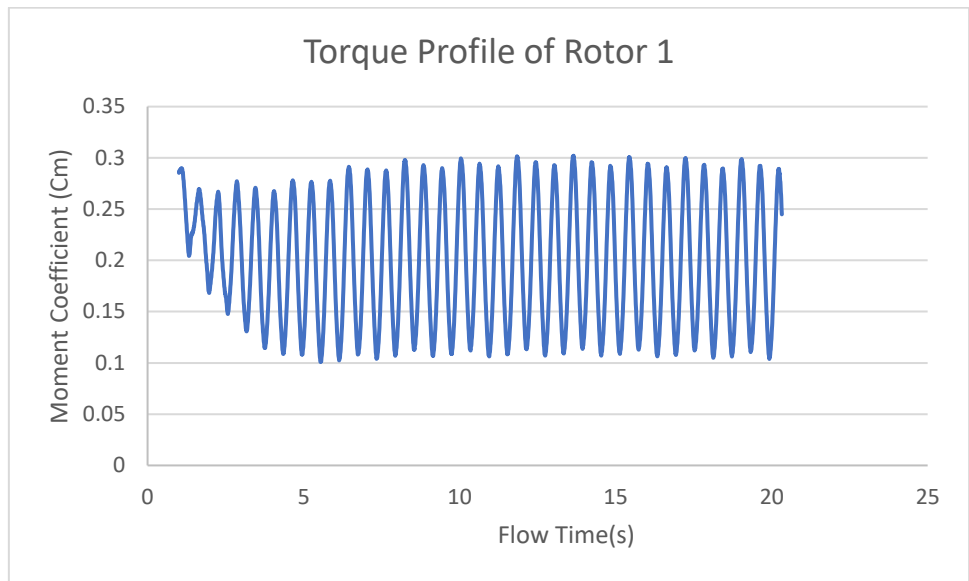Figure 55: Figure shows the Vorticity profile of the configuration under consideration.

Figure 56: Torque profile experienced by rotor 1 over the flow time.
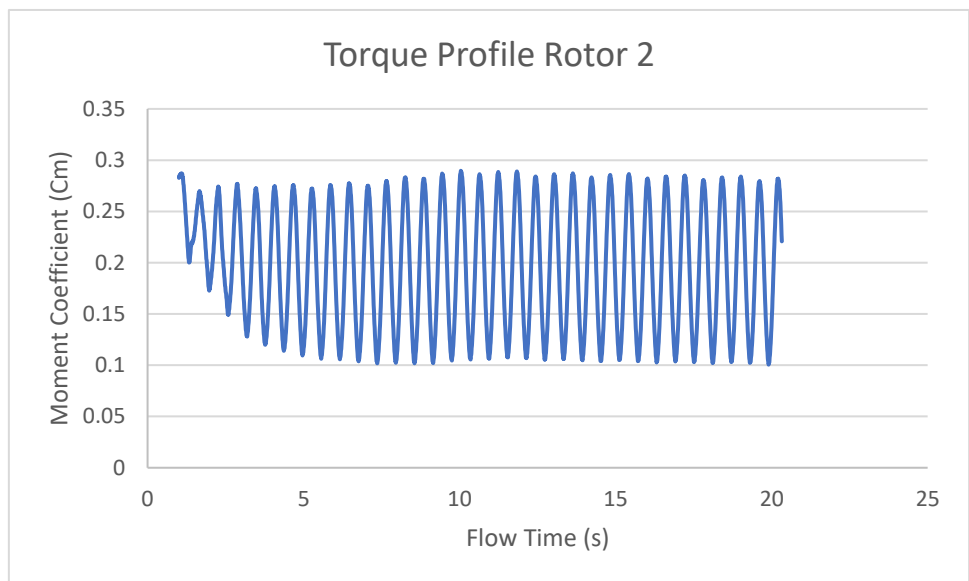

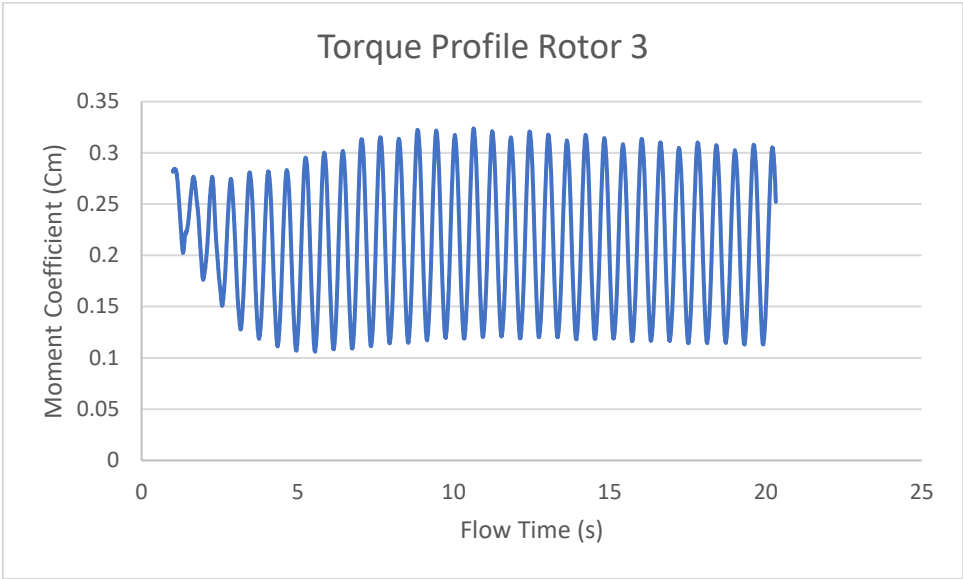Figure 57: Torque profile experienced by the rotor 2 over the flow time.

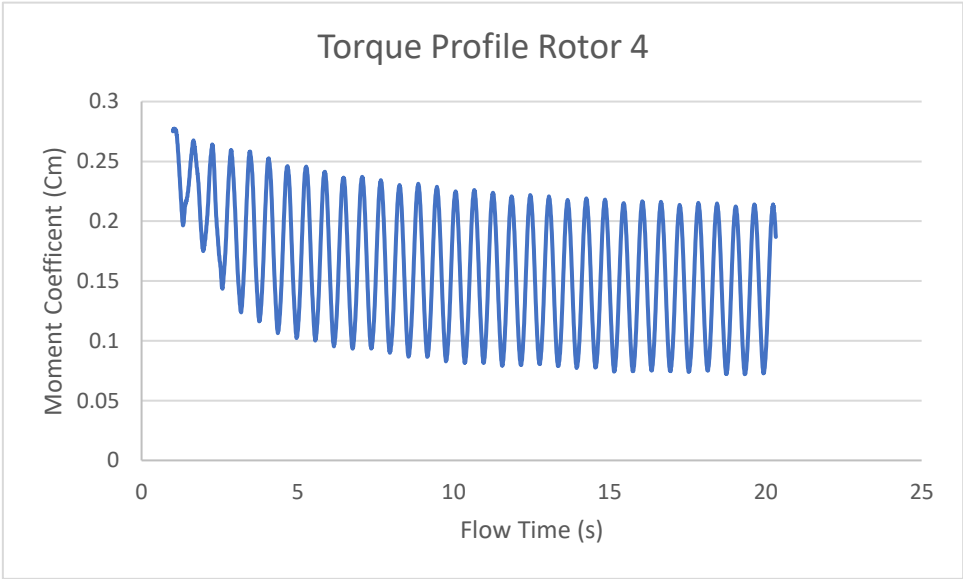Figure 58: Torque profile experienced by rotor 3 over the flow time.

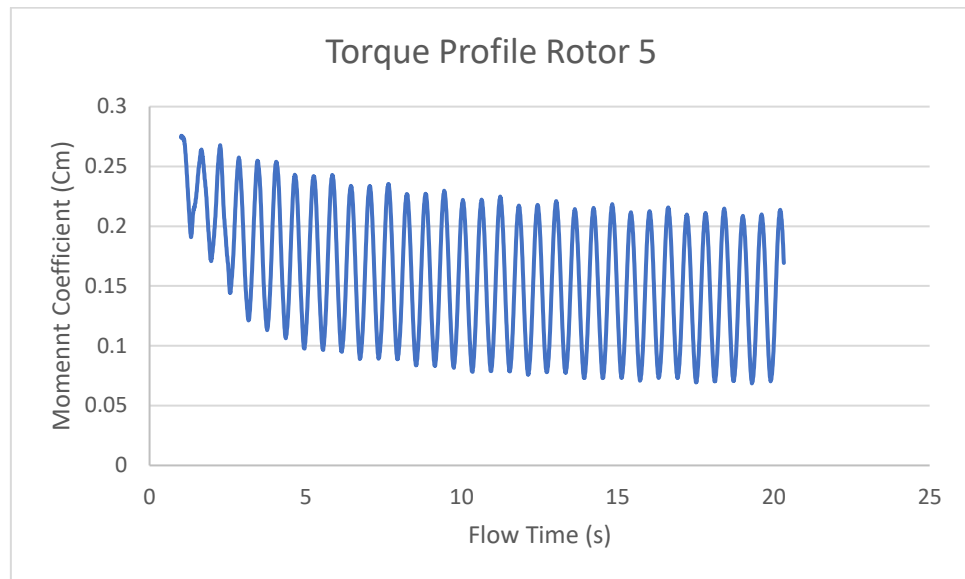Figure 59: Torque profile experienced by the rotor 3 over the flow time.

Figure 60: Torque profile experienced by rotor 3 over the flow time.

Figure 56,7, 58,59,60 shows the torque profile experienced by the rotor 1,2,3,4,5 respectively. over the flow time. Figure 54 shows the distribution of the rotors arranged in the array and how they are numbered. It is important to number the rotor in order to identify the performance of each to the performance of the system. he increase in efficiency of 34 % for a rhombus system has encouraged the thought of placing one more rotor making it a five-rotor system with staggered configuration. Simulations were performed using a five-rotor system, as shown in figure 53. The configuration yielded a performance coefficient of 1.46. The average moment Coefficient value was 0.208 and the average power coefficient was 0.728 for rotor 1. The average moment Coefficient value was 0.205 and the average power coefficient was 0.717 for rotor 2. The average moment Coefficient value is 0.22 and the average power coefficient is 0.77 for rotor 3. The average moment Coefficient value is 0.168 and the average power coefficient is 0.588 for rotor 4. The average moment Coefficient value was 0.167 and the average power coefficient was 0.588 for rotor 5. The performance of the third rotor has increased as explained earlier, rotor 3 had good performance characteristics, this has led to the overall

increase in performance indicator of 46%. Figure 48 shows clearly how the Moment Coefficient increased and reached an average value of 0.22, highest for an individual rotor so far. It was clear that introducing rotor 4 in the system of a rhombus (Performance indicator =1.34) has led to an increase of 46 %. An additional 12% increase was obtained by the introduction of one more rotor.

The vortex profile of the configuration under consideration is shown in figure 55. Multiple rotors operating in proximity can cause turbulence, vortex shedding, and interference effects such wake interactions. The wake tail may compress as a result of these interactions or behave differently than it would with a single rotor. Multiple rotors also enhance the effective solid blockage area, or the area of the flow area occupied by the rotor blades, which has a positive impact on blockage. The increased obstruction may affect the flow patterns resulting in compression of wake fields. With more rotors in the farm, the obstruction effect becomes more noticeable. A rotor's wake takes some time to recover and return to its original, undisturbed form. The space available for wake recovery in a VAWT farm may be constrained by the closeness of the rotors. Due to this restriction, the wakes may interact more and compress more quickly.

The highest efficiency here is for Rotor 3. In this case farm's performance may benefit from symmetry, especially in respect to the wake field created by the turbines, compared to a four-rotor system. The wake fields generated by symmetrically positioned turbines may be more consistent and uniform. This can reduce wake interference, which happens when downstream turbines experience turbulent or slower wind as a result of an upstream turbine's wake. The VAWT farm's total performance can be enhanced by eliminating wake interference since each turbine can run in a more reliable wind flow in

a synchronized manner. As we can see in the velocity contour the patterns produced by the wake fields are in a symmetrical and synchronized manner for the five-rotor system [51][52][53][54][55]
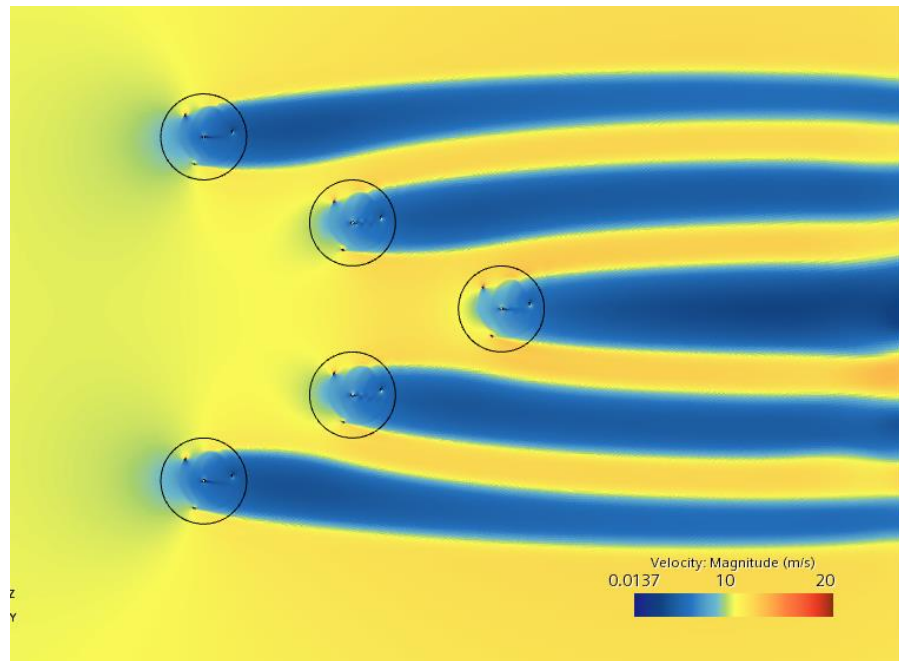
Figure 61: Figure shows the Velocity profile of the configuration under consideration.

Figure 62: Distribution of the rotors are arranged in the array and how they are numbered,

it is important to number the rotor in order to identify the performance of each to the performance of the system. Here in this case, there are five rotors, like an arrow placed at an angle of $60°$
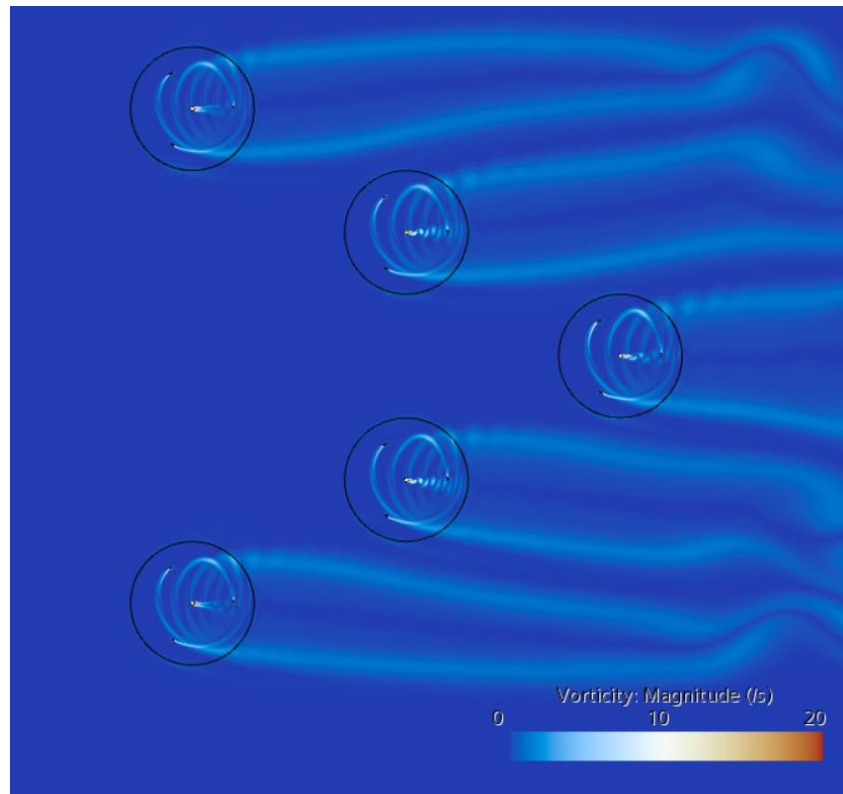

Figure 63: Figure shows the Vorticity profile of the configuration under consideration
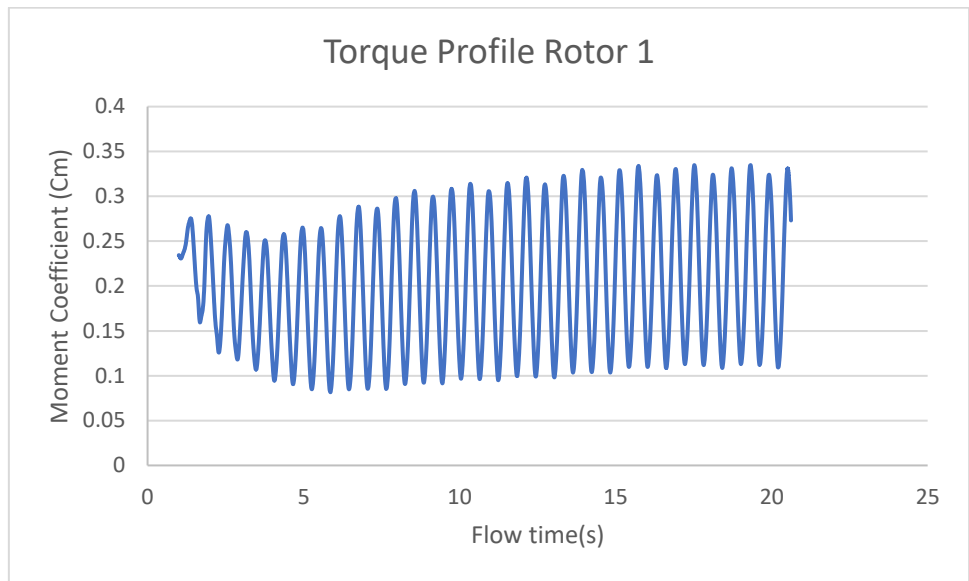
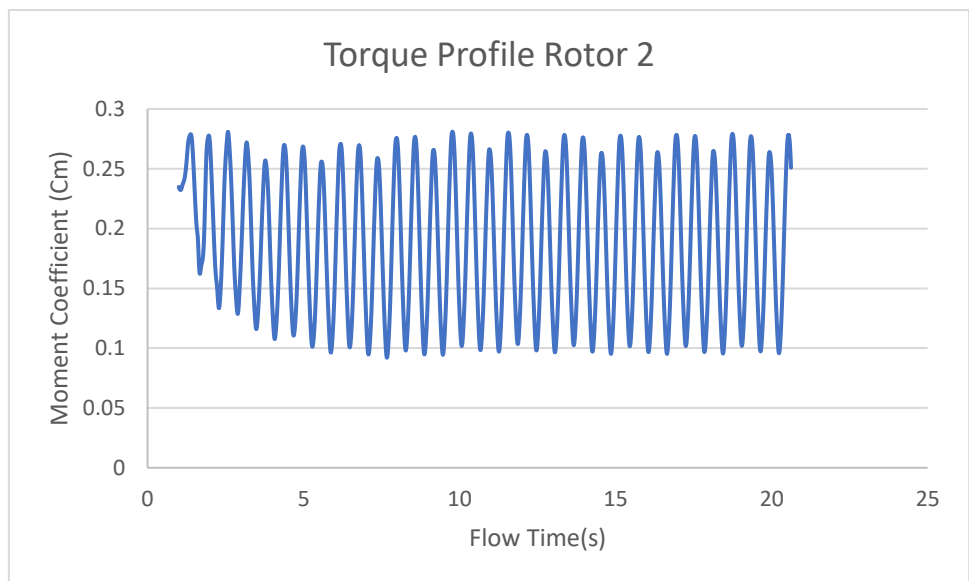Figure 64: Torque profile experienced by rotor 1 over the flow time.

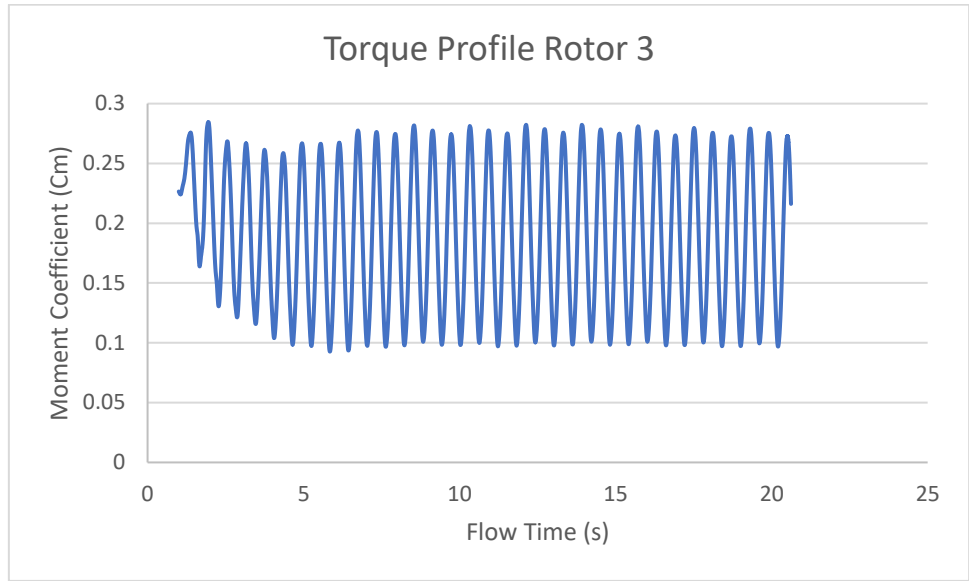Figure 65: Torque profile experienced by the rotor 2 over the flow time.

Figure 66: Torque profile experienced by the rotor 3 over the flow time.
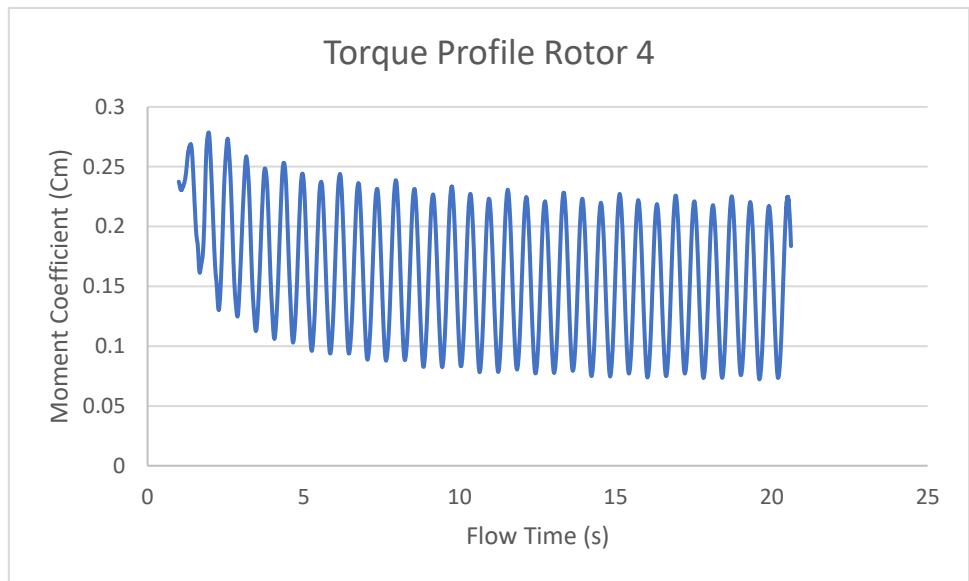
Figure 67: Torque profile experienced by the rotor 4 over the flow time.
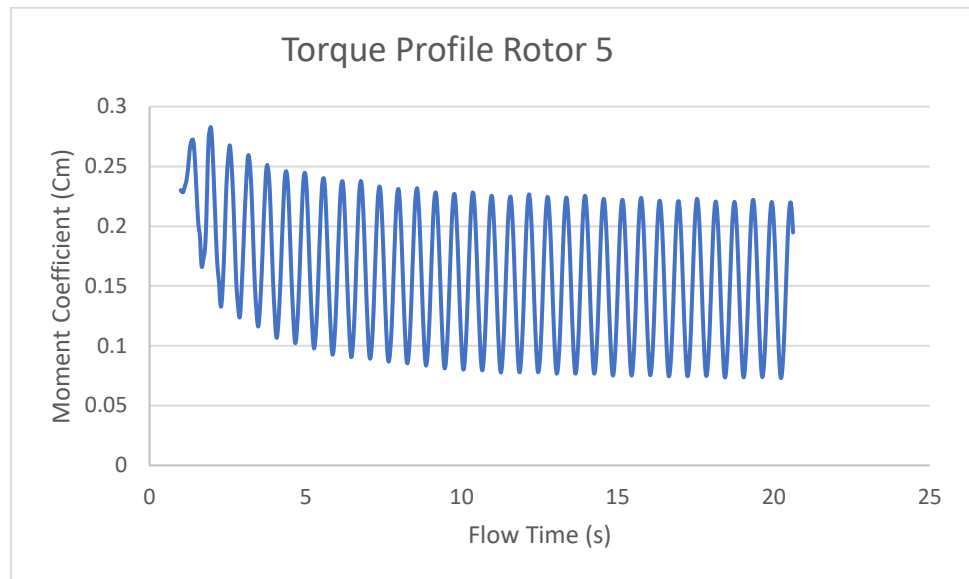
Figure 68: Torque profile experienced by rotor 5 over the flow time.
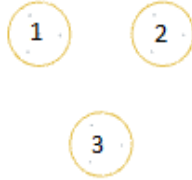
Figure 62 shows the distribution of the rotors arranged in the array and how they are numbered. It is important to number the rotor in order to identify the performance of each to the performance of the system. Here in this case, there are five rotors, like an arrow placed at an angle of 60°. Figure 64,65,66,67,68 shows the torque profile experienced by the rotor 1,2,3,4,5 respectively over the flow time.
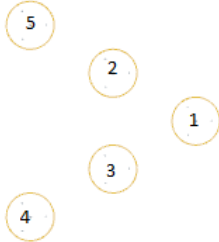
By referring to [12]and considering the increase in efficiency so far due to the converging effect, a V-shaped configuration consisting of five rotors was simulated. The configuration produced a performance coefficient of 1.43. The increase in performance is due to the venturi effect, which led to the increase in performance of the last rotor (R1) compared to the rotors at the middle (R2, R3). The increased velocity near the blades of the final rotor increased the torque, which in turn increased the efficiency of the whole system. The average moment Coefficient value was 0.211 and the average power coefficient was 0.738 for rotor 1. The average moment Coefficient value was 0.195 and the average power coefficient is 0.682 for rotor 2. The average moment Coefficient value is 0.195 and the average power coefficient is 0.682 for rotor 3. The average moment Coefficient value is 0.169

and the average power coefficient is 0.59 for rotor 4. The average moment Coefficient value was 0.168 and the average power coefficient was 0.59 for rotor 5. The performance of R1 has increased, this has led to the overall increase in performance indicator of 43%. Figure 53 shows clearly how the Moment Coefficient increased and reached an average value of 0.211. R2 and R3 have similar moment and power coefficient values, similarly R4, R5 have similar characteristics, this may be due to the symmetry of the simulation.

Table 6: Table showing the values of Moment Coefficient (Cm) and Power Coefficient (Cp) at different configurations.

Configuration	Rotor	Moment Coefficient (Cm)	Power Coefficient (Cp)
Rotor in isolation	1	0.137	0.479
Two Rotor	1	0.138	0.472
	2	0.159	0.54
Three Rotor	1	0.153	0.535

  1 2 3	2	0.163	0.57
	3	0.153	0.535
Three Rotor with blockage 1 2 3	1	0.145	0.507
	2	0.058	0.203
	3	0.184	0.644
Four rotors with blockage 1 4 3 2	1	0.171	0.598
	2	0.183	0.64
	3	0.0712	0.249
	4	0.0862	0.301
Four Rotors	1	0.154	0.539
	2	0.173	0.60

	3	0.2057	0.717
	4	0.190	0.665
Five Rotor Staggered	1	0.208	0.728
	2	0.205	0.717
	3	0.22	0.77
	4	0.168	0.588
	5	0.167	0.588
Five rotor arrows	1	0.211	0.738
	2	0.195	0.682
	3	0.195	0.682
	4	0.169	0.59

	5	0.168	0.59

Table 7: Table showing the values of Performance coefficient at different configurations.

Array Configuration	Performance indicator(Ω)
Rotor in isolation	1
Two rotor	1.054
Three rotors	1.14
Three rotors with blockage	0.96
Four Rotors	1.34
Four rotors with blockage	0.933
Five Rotors Staggered	1.466
Five rotors arrow	1.43

4.6   Comparison of CPU Time
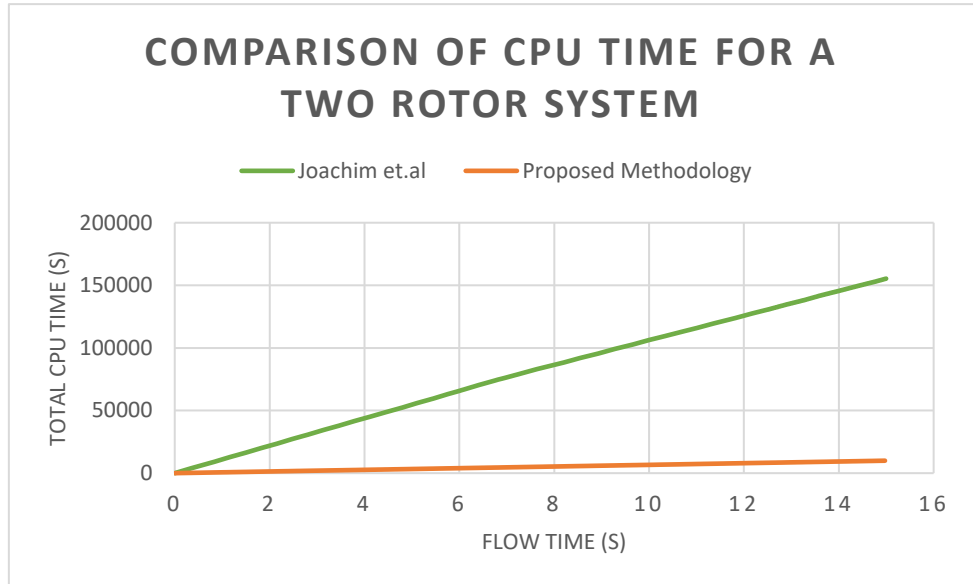
Figure 69: Comparison of CPU time for [15] Hansen et.al. and the Proposed

methodology for a two-rotor system.
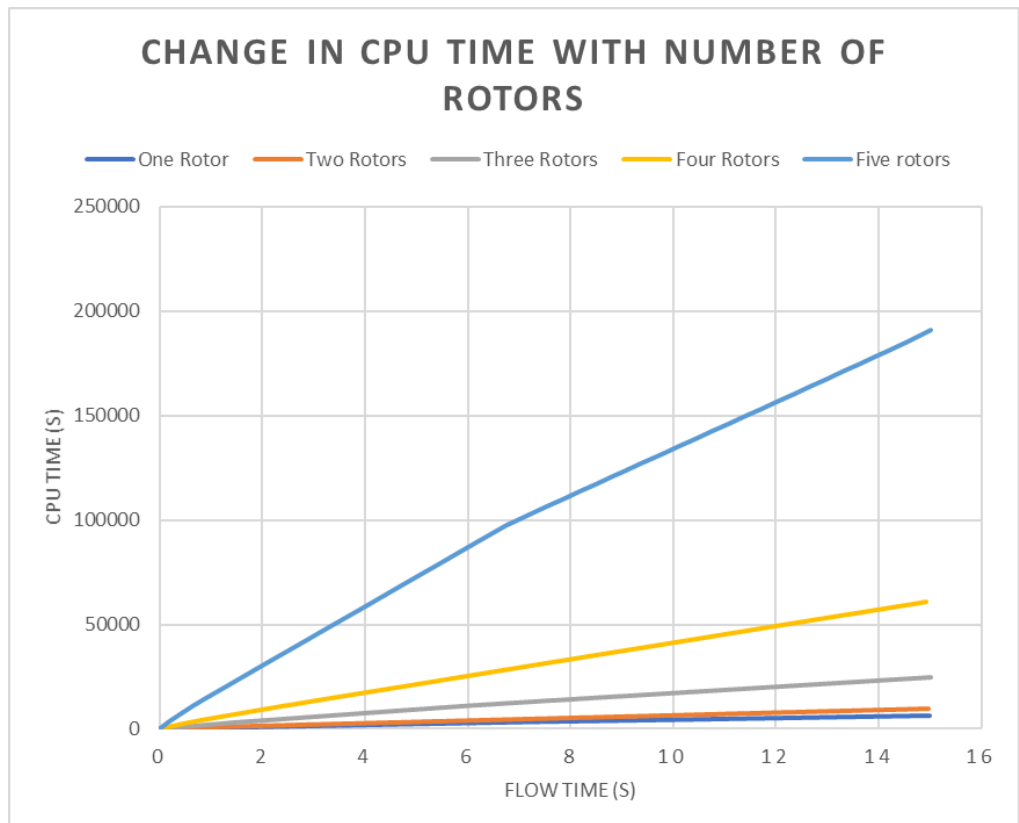
Figure 70: Change in Computational Time with increase in number of rotors in the system.

Comparison of CPU time for various configurations proved that the proposed methodology can be computationally feasible for multiple rotors. Figure 69 shows the comparison of CPU time for [15] Hansen et.al. and the Proposed methodology for a two-rotor system. When the number of rotors increases the CPU time also tends to increase exponentially as finer meshes are needed near the rotor blades. Therefore, the number of finer grids needed for computation also increases which in turn increases the computational time. This makes the methodology followed by [15] Hansen et.al computationally expensive for multiple rotor systems. The proposed methodology reduces the CPU time to a great extent. The CPU hours for simulating 17 complete revolutions (30 seconds of flow time) of a rotor in isolation was approximately 3.5 hours. The Change in Computational Time with increase in number of rotors in the system shown in Figure 70

5. Discussion

After the series of simulations done on VAWT it was evident that the more sensible configurations cab yields improved efficiency. The discussions given below will analyze the results produced, the reason behind the result and eventually the physics that led to the results.

The main outcome of the simulations were the velocity profiles, computational time and the moment coefficient. The moment coefficient is then converted into power coefficient using the Eq.9 and the performance indicator can be found out from the power coefficient using Eq 10. The results were plotted in table 6 and table 7. The results produced by [15] Hansen et.al clearly indicated that the configuration with 60 produced the best results for a VAWT farm field. Therefore, different configurations involving the same angle and incorporating a

greater number of rotors were tried as from an industrial perspective, it was important to know how the rotors might behave in cluster.

As shown in table 4 at first a rotor in isolation was tried as a benchmark to the other studies and to compare the computational time with other methodologies, it was found that computational time got reduced by a great extent, for the same computational system the computational tie was only 10% of the earlier study done by [15] Hansen et.al. This was due to the reduction in domain size and the changes made in boundary condition (explained in methodology section), the time of computation got reduced without reducing the accuracy. The torque profile was also validated and found similar to the previous studies.

A two-rotor system was tried after that. The second rotor was placed at 2D and at an angle of 60˚. The performance indicator value for the combined two rotor system was about 1.054. This slight increase in performance led to the thought of introducing a three-rotor system in a converging configuration rather than a diverging one in order make use of the venturi effect. which results in the reduction of area and increase in the velocity, this has improved the performance coefficient to value of 1.14. this encouraged to place another rotor like Rhombus with four rotors. The rhombus with four rotors (configuration 5) produced an increase in efficiency of 34%. This paved the way to introduce one more rotor making it a five rotors system with staggered configuration (configuration 7), which led to an improvement in efficiency of 46%. The ideas introduced by [12] and the results from the current study encouraged to place 5 rotors like an arrow at 60˚, which resulted in an improvement of 43%.

The staggered and arrow configuration yielded the most efficiency, the improved results may be due to the venturi effect, which led to the increase in velocity near the vicinity of the blades due to the positioning

of the turbines to enhance the performance of each other. It is more economical to consider the different configuration with the three bladed system to improve the efficiency of the turbine farm rather than to vary the chord length or change the number of rotors which will lead to an increase in manufacturing and installation cost.

It was also found that placing a turbine colinear to each other in the direction of wind can decrease the performance by a great extent. This is due to the fact that the low velocity wake field from one turbine will directly overlap on the other reducing the torque by a great margin. Thus, the rotors of the particular turbine become almost idle. The wind turbines are aligned with the wind direction and their axis of rotation is parallel to the wind direction in a horizontal axis wind turbine (HAWT) farm arrangement. This indicates that there is no considerable restriction or narrowing of the flow route, and the wind passes directly through the rotor or blades of each turbine. This alignment prevents the Venturi effect from being seen and prevents the airflow around the HAWT blades from becoming constrained. On the other hand, the turbines in a farm of Vertical Axis Wind Turbines (VAWT) have a vertical axis of rotation. As a result, the wind and the turbine interact differently. While the Venturi effect does affect VAWTs, other elements also play a part in the power density augmentation that has been seen. In VAWTs, the Venturi effect happens because the flow path between the blades narrows, increasing the local flow velocity. As a result, the flow has more kinetic energy, which might improve the power density.

Field-Flow Interactions: The geometry of the turbine, the topography nearby, the wind speed, and turbulence are only a few of the numerous variables that affect the flow field around a wind turbine. Complex interactions between the rotor and the wake left by the blades in VAWTs define the flow field. These interactions may have an impact

on nearby turbine performance and contribute to the observed power density augmentation.

Wake Effects: The area downstream of a wind turbine where the wind speed is lowered, and turbulence is enhanced is referred to as the wake. The performance of turbines positioned in the wake's downstream zone is significantly impacted. In VAWTs, the intricate interactions between the flow field can alter the wake dynamics, potentially changing the turbine's overall performance.

Discrepancies in Turbine Performance: Performance variations may be caused by variations in turbine position and arrangement. The flow field and the effectiveness of turbines can vary greatly depending on the location, as can factors like wind speed, wind shear, barriers, and neighboring turbines. [52][53][54][55]

In addition to this symmetry also plays a role in the efficiency of the VAWT farm as explained in 5 rotor staggered configuration.

6. Conclusions

The aim of the project was to develop a VAWT CFD simulation which is industrially feasible (incorporating a greater number of rotors in the domain), proposing the best methodology to do the same by reducing the computational cost and time and last but not the least to propose the best VAWT layout. All the aims were fulfilled, and the following conclusions were drawn.

• A number of 2D CFD models were analyzed to find the most efficient configurations and efforts were also made to identify the flow physics behind the increase in efficiency.

- A V shaped five-rotor and a Staggered configuration system produced maximum efficiency (performance improved by 43% an 46% respectively). This may be due to the venturi effect produced by the different layers of turbines placed to improve the performance of the final rotor without compromising its own performance.

- From an industrial point of view, it would be more economical to consider the different configuration with the three bladed system to improve the efficiency of the turbine farm rather than to vary the chord length or change the number of rotor blades which will lead to an increase in manufacturing and installation cost.

- A new methodology has been proposed using a sliding mesh and volume controlled polyhedral meshing approach. The CPU hours for simulating 17 complete revolutions (approximately 30 seconds of flow time) of the rotor was 91 hours for [15] Hansen et.al. was 9.5 hours for the proposed methodology (11th Gen Intel(R) Core (TM) i9-11900K @ 3.50GHz, 3504 Mhz, 8 Core, 16 Logical Processor). The CPU hours were reduced by 90%. It can be concluded that the current study reduces the computational time to a great extent without compromising on the accuracy. This makes the proposed methodology computationally inexpensive and faster compared to the earlier one.

As a suggestion for future work, it would be interesting to observe how the configuration will perform considering the wind direction from different angles. For example, wind can be assumed to blow from west to east, east to west, north to south and south to north. These four situations can be simulated and the average value of these four simulations will give a clearer picture of performance increase rather than wind blowing in a single direction.

7. Reference

[1] D. Brownstein, M. Kinzel, and J. O. Dabiri, "Performance enhancement of downstream vertical-axis wind turbines," J. Renew. Sustain. Energy, vol. 8, no. 5, p. 053306, Sep. 2016.

[2]S.H.Hezaveh, E. Bou-Zeid, J. Dabiri,M. Kinzel, G. Cortina, and L.Martinelli, "Increasing the Power Production of Vertical-Axis Wind-Turbine Farms Using Synergistic Clustering," Boundary-Layer Meteorol., vol. 169,no. 2, pp. 275–296, Nov. 2018.

 [3] S. Zanforlin and T. Nishino, "Fluid dynamic mechanisms of enhanced power generation by closely spaced vertical axis wind turbines," Renew. Energy, vol. 99, pp. 1213–1226, Dec. 2016.

[4] G. Mosetti, C. Poloni, and B. Diviacco, "Optimization of wind turbine 552 positioning in large windfarms by means of a genetic algorithm," 1994. 553.

[5] Tang, H.; Lam, K.-M.; Shum, K.-M.; Li, Y. Wake Effect of a Horizontal Axis Wind Turbine on the Performance of a Downstream Turbine. Energies 2019, 12, 2395

[6] J. O. Dabiri, "Potential order-of-magnitude enhancement of wind farm power density via counter-rotating vertical-axis wind turbine arrays," J. Renew. Sustain. Energy, vol. 3, no. 4, p. 043104, Jul. 2011.

[7] R. W. Whittlesey, S. Liska, and J. O. Dabiri, "Fish schooling as a basisfor vertical axis wind turbine farm design," Bioinspir. Biomim., vol. 5, no. 3, p. 035005, Sep. 2010.

[8] Letcher, T. M. (2017) Wind energy engineering: a handbook for onshore and offshore wind.

[9]Dabiri, J. O. (2011) 'Potential order-of-magnitude enhancement of wind farm power density via counterrotating vertical-axis wind turbine

arrays', Journal of renewable and sustainable energy, 3(4), pp. 043104.turbines. London: Academic Press.

[12] Determining the Impact of VAWT Farm 1Configurations on Power Output 23 Andrew Barnes*, Ben Hughes

[13] Eriksson, S., Bernhoff, H. and Leijon, M. (2008) 'Evaluation of different turbine concepts for wind power', renewable and sustainable energy reviews, 12(5), pp. 1419-1434.

[14] Wu YT, Porté-Agel F (2012) Atmospheric turbulence effects on wind-turbine wakes: an LES study. Energies 5(12):5340–5362.

[15] Hansen et.alJoachim Toftegaard Hansena, Mahak Mahak, IakovosTzanakis. Numerical modelling and optimization of vertical axis wind turbine pairs: A scale up approach. Renewable Energy Volume 171, June 2021, Pages 1371-1381.

[16] S. H. Hezaveh, E. Bou-Zeid, J. Dabiri, M. Kinzel, G. Cortina, and L. Mar528 tinelli, "Increasing the Power Production of Vertical-Axis Wind-Turbine Farms Using Synergistic Clustering," Boundary-Layer Meteorol., vol. 169, no. 2, pp. 275–296, Nov. 2018.

[17] N. Bons, "Optimization of Vertical Axis Wind Turbine Farm Layout," 554 Am. Inst. Aeronaut. Astronaut., pp. 1–8.

[18] Brownstein, I.D.; Wei, N.J.; Dabiri, J.O. Aerodynamically Interacting Vertical-Axis Wind Turbines: Performance Enhancement and Three-Dimensional Flow. Energies 2019, 12, 2724.

[19] Shamsoddin, S.; Porte-Angel, F. Large Eddy Simulation of Vertical Axis Wind Turbine Wakes. Energies 2014, 7, 890–912.

[20] Bremseth, J.; Duraisamy, K. Computational analysis of vertical axis wind turbine arrays. Theory. Comput. Fluid Dyn. 2016, 30, 387–401

[21] "Wind Energy Explained: Theory, Design and Application" by Anthony L. Rogers, James F. Manwell, and Jon G. McGowan.2009

Dayong Gao and Ramesh K. Agarwal wrote "Vertical Axis Wind Turbines: A Review" [22 Year: 2018 Energies, 11(8), 2033. DOI: 10.3390/en11082033

[23] "Analysis and improvement of aerodynamic performance of straight bladed vertical axis wind turbines," Ahmadi-Baloutaki, M. (2015).

[24] Smith, A., et al., "Horizontal axis wind turbine performance in high-wind areas." 75, 123 – 135 of the Renewable Energy Journal.

[25] Anderson, C., Johnson, B. (2018). Journal of Wind Engineering and Industrial Aerodynamics, 189, 45 – 56. "Evaluation of wind turbine performance in high-wind sites."

[26] D. Chen et al., 2019. "Analysis of wind turbine performance under high-wind conditions." Journal of Energy Conversion and Management, 196, 123-137.

[27] Performance evaluation of low wind speed horizontal and vertical axis wind turbines. Volume 76, Pages 133 – 141, Pournaras, M. Negnevitsky, and V. G. Agelidis (2015).

[28] Authors: M. B. Bannikov, V. A. Pilipenko, and A. Yu. Borisov; 2017 International Conference on Industrial Engineering, Applications, and Manufacturing (ICIEAM); Design and performance study of an adva vertical axis wind turbine.

[29] J. R. Holton (2004). A Survey of Dynamic Meteorology. University Press."The Equations of Motion in Spherical Coordinates" is Chapter 4's subject.

[30] (2006) Wallace, J. M., and Hobbs, P. V. A Basic Survey of Atmospheric Science. University Press."The General Circulation of the

Atmosphere" is the subject of Chapter 6.

[31] United States Department of Energy. "Smaller Vertical Axis Wind Turbines." on the Energy.gov website at: https://www.energy.gov/eere/wind/small-vertical-axis-wind-turbines

[32] Bruce Tullis, "Vertical Axis Wind Turbines: Great in 1890, Also-rans in 2014." World of Renewable Energy.

[33] Jadhav, M. M. Malik, and Aniket M. Review of Vertical Axis Wind Turbine Design and Development. Volume 3, Number 5, May 2013, International Journal of Emerging Technology and Advanced Engineering.

[34] Resch, B.P., and M.D. Prickett (2009). Yaw controls to enhance wind turbine energy absorption. 97(10-11), 542-552 in Journal of Wind Engineering and Industrial Aerodynamics.

[35] The report is from the International Renewable Energy Agency (IRENA) and is titled "Renewable Energy Technologies: Cost Analysis Series - Wind Power." (2012)

Written by David A. Spera, "Wind Turbine Technology: Fundamental Concepts of Wind Turbine Engineering" (p. 36). 2010

[37] Godfrey Boyle's book "Renewable Energy: Power for a Sustainable Future"2012

[38] Vimal et al. 2017, Velocity and performance correction methods for hydrokinetic turbines explored with variable channel shape Energies 14(4):996

[39] Hu et al.'s 2017 study, "Performance Analysis of Asymmetric Airfoils for Vertical Axis Wind Turbines." 14(4):996 in Energies.

[40] B. Alipanah and S. Soltani (2018), "Volume 173, Pages 1-11,"

Journal of Wind Engineering and Industrial Aerodynamics.

[41]Ahlström, K., Larsson, J., and Jensen (2012) are references. Comparison of wind turbines with three and four blades. European Wind Energy Association 2012 Conference & Exhibition Proceedings

[42] Srensen, J. N. (2011), Aerodynamics of Wind Turbines, 2nd ed. Earthscan. [43] Bossanyi, E., Jenkins, N. Sharpe, & T. Burton (2011). (2) Wind Energy Handbook. Wiley.

[43] Jenkins, N. Sharpe, T. Burton, and E. Bossanyi (2011). (2) The Handbook of Wind Power. Wiley

[44] Fundamentals of Aerodynamics, Fifth Edition [44], J. D. Anderson (2011). McGraw-Hill

[45] Patrick Irungu Muiruri and Oboetswe Seraga Motsamai validated three-dimensional CFD simulations of a wind turbine blade section in the journal of engineering science and technology in February 2018.

find a reasonable balance between computational efficiency and precision.

[46] Zhang H., Jiao X., Chen J., and Liu T. (2018). creation of polyhedral meshes for complicated, large-scale designs. 371, 456-479, Journal of Computational Physics

[47] (2014) Owen S. J., Dohrmann C. R., and Akin J. E. a technological review on unstructured mesh generation. 52(2) of the AIAA Journal, 227 – 264.

[48] V. Nelson (2016). Renewable Energy and the Environment: Wind Energy. Presses CRC.

[49] Yang, S. C., Lu, J. H. (2017). Wind turbines with a vertical axis: theory, design, and application. Springer.

[50] Liu, H., Liu, Y., and Chen, X. investigation on the power

coordination of wind farm clusters. 1421 – 1431 Applied Energy, 231.

[51] In 2019, Mittal, G., and Kumar, B. Review of the Wake Dynamics and Structure of Vertical Axis Wind Turbines. 10.3390/en12061117. Energies, 12(6), 1117.

[52] (2015) Saha, U., and Prasad, M. Analysis of the power output of a wind turbine with a vertical shaft operating under Indian atmospheric conditions. 859 – 868. Renewable Energy, 83.

[53] (2016). Bastankhah, M., and Porté-Agel, F. Wind turbine waves under yawed situations are the subject of experimental and theoretical research. 806, 506-541, Journal of Fluid Mechanics.

[54] L. P. Chamorro and F. Porté-Agel (2011). A large-eddy simulation investigation of the effects of atmospheric stability on wind-turbine wakes. Fluid Physics, 23(4), 045102.

[55] Churchfield, M. J.; Lee, S.; and Moriarty, P. J. (2012). In the setting of a yawed wind farm, a large-eddy simulation investigation of wake meandering and impacts on turbine loads. 225-241 in Wind Energy, 15(2).

[56] A. J. Chorin (1968). Navier-Stokes Equations Numerical Solution. 745-762 in Mathematics of Computation, 22(104).

[57] Shin, C. T., Ghia, U., and Ghia, K. N. (1982). Using a multigrid approach and the Navier-Stokes equations, high-Re solutions for incompressible flow are provided. 48(3), 387-411, Journal of Computational Physics.

[58] Ferziger, J. H., and Peri, M. methodologies for fluid dynamics computation. Science & Business Springer.